

STRATIGRAPHY AND GEOCHEMICAL CHARACTERISATION OF UPPER CRETACEOUS NON-MARINE – MARINE CYCLES (GRÜNBACH FORMATION, GOSAU GROUP, AUSTRIA)

Gerald HOFER¹⁾, Erich DRAGANITS¹⁾²⁾, Michael WAGREICH¹⁾, Christa-Charlotte HOFMANN³⁾, Doris REISCHENBACHER⁴⁾, Marie-Louise GRUNDNER¹⁾ & Magda BOTTIG⁵⁾

¹⁾ Department of Geodynamics and Sedimentology, University of Vienna, Althanstrasse 14, A-1090 Vienna, Austria;

²⁾ Department of Prehistoric and Medieval Archaeology, University of Vienna, Franz-Klein-Gasse 1, A-1190 Vienna, Austria;

³⁾ Department of Palaeontology, University of Vienna, Althanstrasse 14, A-1090 Vienna, Austria;

⁴⁾ Department of Applied Geological Sciences and Geophysics, Montanuniversität Leoben, Franz-Joseph-Strasse 18, A-8700 Leoben, Austria;

⁵⁾ Geological Survey of Austria, Neulinggasse 38, A-1030 Vienna, Austria;

¹⁾ Corresponding author, gerald.hofer@univie.ac.at

KEY WORDS

Early Campanian
Stable Isotopes
Geochemistry
Gosau Group
Coal cycles
Palynology
Boron

ABSTRACT

Early Campanian non-marine – marine cycles of the Grünbach Formation (Gosau Group, Northern Calcareous Alps, Austria) within the Grünbach Syncline have been investigated using sedimentology, micropaleontology and geochemistry. The succession of the Grünbach Formation comprises clay, marl, siltstone, sandstone as well as rare conglomerate and coal beds deposited in a marginal marine to terrestrial, brackish-limnic environment. Sampling was done from a 45 m section of an artificial trench at Maiersdorf, Lower Austria. Palynological data indicate quite warm and humid depositional conditions. The observation of *Nypa* pollen represents the northernmost occurrence known so far from the Campanian. Based on geochemical proxies (whole rock geochemistry and bulk carbon and oxygen isotopy) as well as microfossil data, five marine (MC1-5) to non-marine cycles (NC1-5) are reconstructed. Marine intervals were identified basically by the presence of nannofossils and by higher mean $\delta^{13}\text{C}$ ratios (-4.51 VPDB), boron contents (mean 165.8 ppm) and B/Al* ratios (mean 167.2) compared to sections interpreted as non-marine (mean $\delta^{13}\text{C}$: -6.34 VPDB, B: 139.0 ppm, B/Al*: 149.4). A statistically significant differentiation between marine and non-marine samples is possible using the aluminium-normalized boron ratio and, to a lower degree, the absolute boron values. A duration of a few 100 kyrs is estimated for single non-marine – marine cycles. Low subsidence rates and uniform provenance data argue against a purely tectonic origin of the cycles and are in favor for a mainly climatic control of these transgressive-regressive cycles in the Early Campanian.

Nichtmarin-marine Zyklen im Frühen Campanium der Grünbach-Formation (Gosau-Gruppe, Nördliche Kalkalpen, Österreich) innerhalb der Grünbach-Synklinale wurden mit Hilfe sedimentologischer, mikropaläontologischer und geochemischer Methoden untersucht. Die Abfolge setzt sich aus Tonen, Mergeln, Siltsteinen, Sandsteinen sowie seltener aus Konglomeraten und Kohlelagen zusammen und wurde in einem randmarinen bis terrestrischen Milieu abgelagert. Die Beprobung wurde an einem 45 m mächtigen Profil in einem Schurfgraben bei Maiersdorf (Niederösterreich) durchgeführt. Auf der Grundlage von geochemischen Parametern (Gesamtgesteinsschemie und stabile Isotopen des Gesamtgesteins) sowie mikropaläontologischen Daten wurden 5 marine (MC1-5) und nicht-marine (NC1-5) Zyklen rekonstruiert. Marine Intervalle wurden vor allem durch das Auftreten von Nannofossilien identifiziert und sind charakterisiert durch höhere mittlere $\delta^{13}\text{C}$ Verhältnisse (-4.51 VPDB), Borgehalte (Mittelwert 165.8 ppm) und B/Al* Verhältnisse (Mittelwert 167.2) im Vergleich zu nicht-marinen Abschnitten (Mittelwert $\delta^{13}\text{C}$: -6.34 VPDB, B: 139.0 ppm, B/Al*: 149.4). Eine statistisch signifikante Unterscheidung zwischen marin und nicht-marinen Proben ist mit Hilfe der Aluminium-normalisierten Borgehalte möglich und, in einem geringeren Maß, mit den absoluten Borgehalten. Die Zeitdauer einzelner marin – nicht-mariner Zyklen wird auf mehrere hunderttausend Jahre geschätzt. Geringe Absenkungsraten und einheitliche Materialherkunft sprechen gegen eine ausschließlich tektonische Kontrolle der Zyklen und weisen eher auf eine klimatische Beeinflussung dieser transgressiv-regressiven Zyklen im Frühen Campanium hin.

1. INTRODUCTION

The Cretaceous, especially the mid-Cretaceous, constitutes the last long greenhouse phase of the Earth, characterized by high temperatures and a relatively equable climate. Late Cretaceous times were characterized by the long-term change from the mid-Cretaceous super-greenhouse mode to the Cenozoic icehouse mode of the Earth climate system (e.g., Norris et al., 2002; Forster et al., 2007). Short-term climatic and environmental cycles and events become increasingly recognized during this previously inferred equable warm period of

the Cretaceous (e.g., Jenkyns, 2003; Miller et al., 2005a,b, 2008; Wagreich et al., 2011).

Cyclic sea-level changes in the third- to fourth-order time frame are one expression of rapid climate changes, especially during glacial episodes in Earth history (e.g. Ordovician, Carboniferous and Pleistocene) controlled by waning and waxing ice sheets. Recently, also during the Cretaceous such rapid fluctuations of sea-level have been recognized (e.g. Miller et al., 2005a,b; Bornemann et al., 2008).

A critical depositional record for the recognition of sea-level cycles constitutes marginal marine and marine to non-marine cyclic archives including coal cycles (McCabe and Parrish, 1992). We describe a cyclic non-marine – marine record from the Upper Cretaceous Gosau Group of the Northern Calcareous Alps of Austria. The principal aim of the paper is the recognition and definition of the cyclic record by using sedimentological features, geochemical proxies and the microfossil record. Cycles are then discussed in terms of eustatic versus regional tectonic control.

2. GEOLOGICAL SETTING

The Upper Cretaceous-Eocene Gosau Group was deposited unconformably onto folded and faulted Permo-Triassic sediments of the Northern Calcareous Alps (NCA) (Wagreich and Decker, 2001). Widespread erosion and the formation of karst bauxites evidence subaerial exposure before the deposition of the Gosau sediments (Wagreich and Faupl, 1994). Basin analysis indicates a division into a Lower Gosau Subgroup (Upper Turonian to Campanian) with diachronous deposition of continental to shallow marine sediments in only partly connected, fault bounded basins, and an Upper Gosau Subgroup (Santonian/Campanian to Eocene) comprising deep-water sediments (Wagreich, 1993; Wagreich and Faupl, 1994).

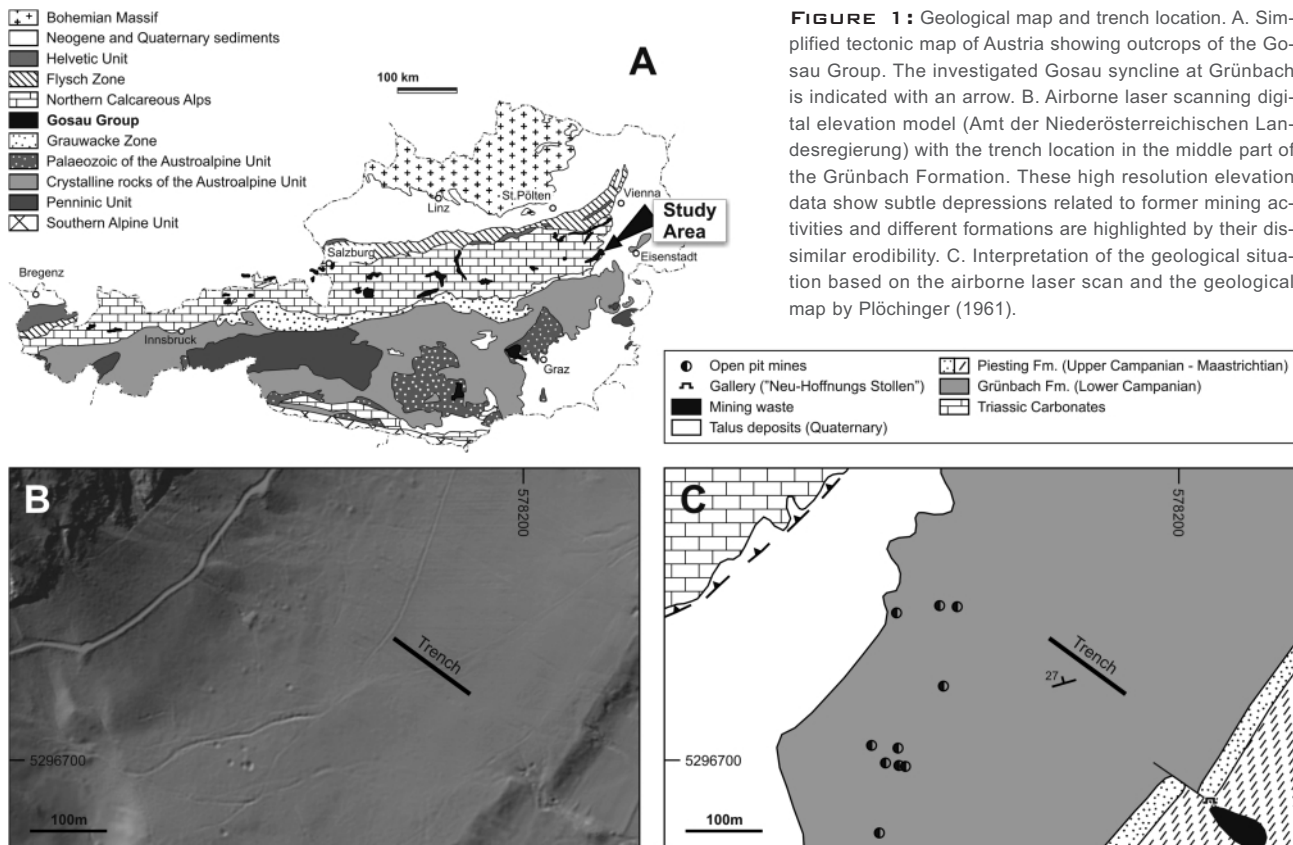
This study investigates Early Campanian terrestrial-marine cycles in one of the easternmost Gosau Group occurrences in the NCA (Fig. 1). The Gosau Group of the Grünbach Syncline (Upper Cretaceous to Paleogene) crops out in a ca. 15 km

long, mainly SW-NE oriented syncline at the transition from the NCA to the southern part of the Vienna Basin, tectonically positioned on southern (higher) tectonic units of the NCA (Plöchinger, 1961). Lithologically the syncline comprises terrestrial conglomerates, sandstones and shallow marine limestones at the base, followed by a siliciclastic succession with up to eight major coal horizons, succeeded by deeper water sandstones, shales, and marls (Plöchinger, 1961; Sachsenhofer, 1987; Summesberger et al., 2007). The total thickness is around 1200 m (Plöchinger, 1961) with a stratigraphic range from the Late Santonian to Paleocene (Summesberger et al., 2007) (Fig. 2).

The general structure of the Grünbach Gosau is a non-cylindrical, tight, inclined, parallel fold, which can be divided into two parts, based on its structures. In the western part the strike of the syncline is more or less W-E with axial surfaces dipping around 60° towards North, while in the eastern part the syncline strikes SW-NE with axial surfaces dipping towards south-east around 60° (Plöchinger, 1961).

2.1 AGE OF THE GRÜNBACH FORMATION

The lithostratigraphy and biostratigraphy of the Gosau Group of the Grünbach Syncline has recently been summarized by Summesberger (1997) and Summesberger et al. (2000, 2002, 2007) indicating deposition of the whole group between the Late Santonian and Paleocene. A latest Santonian to earliest Campanian older age limit of the Grünbach Formation, which is studied here, is constrained by the ammonite *Placenticeras polyposis* (Dujardin) and the inoceramid bivalve *Cordicera-*



mus muelleri Petrascheck from the upper part of the underlying fully marine Maiersdorf Formation (Summesberger et al., 2000). This age is further supported by nannofossils including *Marthasterites furcatus* and *Calculites cf. obscurus* (nannofossil standard zone CC16-17; see Summesberger et al., 2002) and a $^{87}\text{Sr}/^{86}\text{Sr}$ value of 0.707480, indicating an age of 83.3 ± 0.5 Ma, i.e. around the Santonian/Campanian boundary (Scharbert in Summesberger et al., 2002). The Late Campanian younger age limit is constrained by the bivalves *Trochoceramus cf. morgani* (Sornay) and *Trochoceramus cf. dobrovi* Pavlova (Summesberger et al., 2002) and nannofossil data (CC18-22) in lower parts of the overlying Piesting Formation (Summesberger et al., 2002) and by orbitoids from the base of the Piesting Formation (Plöchlänger, 1961, 1967).

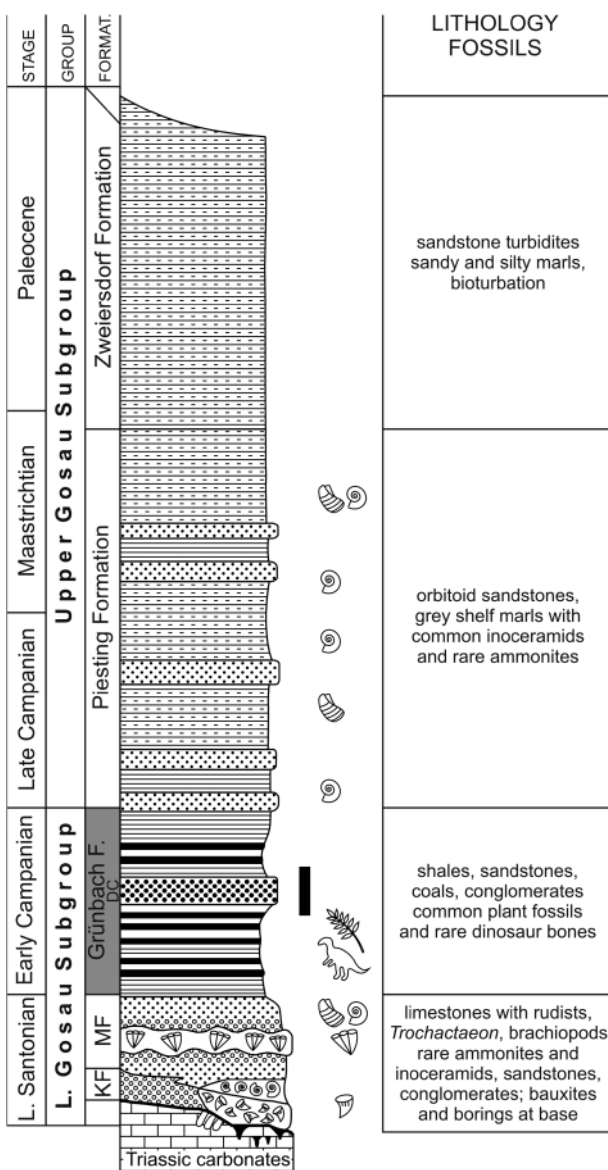


FIGURE 2: Composite stratigraphy of the Gosau Group of the Grünbach Syncline from Piesting to Grünbach (modified after Summesberger et al., 2002, 2007). Thick vertical line to the right of the section indicates the approximate stratigraphic position of the investigated sediments of the trench at Maiersdorf. Abbreviations: KF - Kreuzgraben Formation, MF - Maiersdorf Formation, DC - Dreistetten conglomerate.

3. MATERIALS AND METHODS

Between 1823 and 1965 the Grünbach Syncline has been well-exposed by huge underground and open pit coal mining (Kreiner, 1994) with mining activity down to 1200 m below surface. At present, the outcrop condition worsened dramatically due to the easily weathering lithologies, high precipitation and recultivation. Due to the virtual lack of outcrops and well data in the area of the Grünbach Gosau an artificial trench was dug to expose the coal-bearing cycles. The trench location has been selected based on a compilation of existing literature, geological maps, mining plans and sections in the archives of the Austrian Geological Survey and their integration into a GIS project (Fig. 1).

Excavation and documentation of the up to 4 m deep trench has been carried out between 25 and 28 May 2010 in the cadastre municipality of Grünbach, on a meadow owned by the Agrargemeinschaft Maiersdorf (cadastral register number 845/1) (Fig. 1). The excavation of the trench is oriented perpendicular to the strike of the syncline and started in the Southeast within the overturned limb of the syncline, progressing up-hill towards older strata of the Lower Campanian Grünbach Formation (Fig. 1). Due to the high instability of the trench faces, the trench had to be back-filled immediately after documentation. In total a 141 m long trench has been excavated, exposing almost 45 m of the Lower Campanian Grünbach Formation (Fig. 3).

3.1 SEDIMENTOLOGY

The sedimentology of the trench section was investigated during trench exposure using standard field logging methods, including grain size estimates, bedding and structure identification complemented by thin section analysis from sandstone and conglomerate beds. In total 92 rock samples have been collected for further analyses; they are housed in the sample archive of the Department of Geodynamics and Sedimentology, University of Vienna (for analyzed samples see Online Appendix B). Samples of the trench have been taken between 4 m to 1.5 m below grassroots.

3.2 CALCIUM CARBONATE AND TOTAL ORGANIC CARBON CONTENT

The calcium carbonate content from 55 samples was analyzed using the “Carbonate Bomb” (after Müller and Gastner, 1971) at the University of Vienna. An absolute error of 1% CaCO_3 is given for this method.

Fifty samples were measured for total organic carbon (TOC) with carbon analyzers LECO C200 and LECO RC-412 after dissolving the carbonate with diluted hydrochloric acid (for LECO C200) or measuring at 550°C (LECO RC-412) at the University of Vienna. The accuracy of the measurements is around 0.1%.

3.3 WHOLE-ROCK GEOCHEMISTRY

Thirty-seven fine-grained sediments such as shales, marls and some siltstones were used for the geochemical bulk rock analysis. The chemical analysis was done by the AcmeLabs (Acme Analytical Laboratories Ltd., www.acmelab.com) in Van-

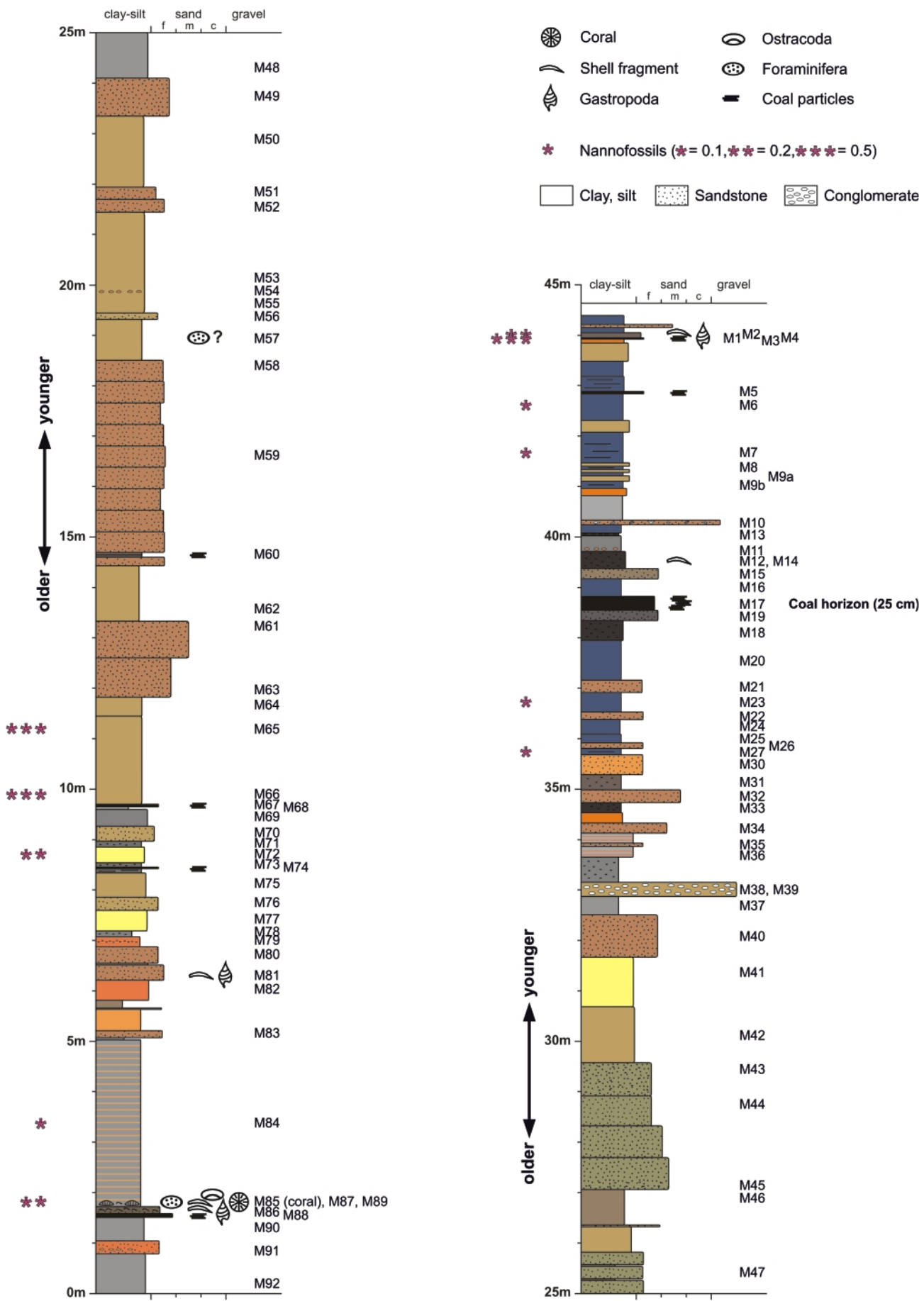


FIGURE 3: Lithostratigraphic section and fossil occurrences of the part of the Grünbach Formation which has been documented in the trench at Maiersdorf (see Figure 1 for location). Bed colours broadly correspond to the rock colours in the field; M1 to M92 are sample numbers.

couver (Canada).

Oxides (SiO_2 , Al_2O_3 , Fe_2O_3 , MgO , CaO , Na_2O , K_2O , TiO_2 , P_2O_5 , MnO and Cr_2O_3) and some minor elements (Ba, Be, Co, Cs, Ga, Hf, Nb, Ni, Rb, Sn, Sr, Ta, Th, U, V, W and Zr) as well as the loss on ignition (LOI) were detected by ICP-emission spectroscopy. For the analysis of trace elements (REE: Sc, Y, La, Ce, Pr, Nd, Sm, Eu, Gd, Tb, Dy, Ho, Er, Tm, Yb and Lu; noble and base metals: Mo, Cu, Pb, Zn, Ni, As, Cd, Sb, Bi, Ag, Au, Hg, Ti and Se) ICP-mass spectroscopy was used. For accuracy, precision and detection limits of these analyses see www.acmelab.com.

Major and trace elements are prevalently used as proxies for the interpretation of paleoenvironments. Boron accumulating in (marine) water is attached in clay minerals (mostly in illites) as well as organic substances and remains relatively immobile. Marine sediments are commonly characterised by higher boron concentrations compared to non-marine sediments. Consequently, boron content is commonly used as a paleosalinity indicator (Ernst, 1966; Heling, 1967; Selter et al., 1989, Rügner, 2000). Unfortunately, grain size and source area of the clays can have additional effects on the boron concentration (Dominik and Stanley, 1993). To reduce these of different grain size and mineralogy, boron contents are normalized to aluminium (multiplied with a factor of 100.000 to get natural numbers). This ratio ($\text{B}/\text{Al}^* \times 100.000$) is used as B/Al^* in the following text.

Discriminant function analysis using major elements to determine provenance signatures is applied to the data set (Roser and Korsch, 1988). Other geochemical indices used include U/Th and TOC/S ratios as well as the chemical index of alteration (CIA) and the chemical proxy of alteration (CPA). The TOC is often used in combination with sulphur (TOC/S-ratio) to infer palaeosalinity of sediments, especially when they are organic rich (Sageman and Lyons, 2004). Generally non-marine sediments are characterised by higher TOC/S-ratios than marine samples with similar TOC contents (Berner and Raiswell, 1984). The chemical index of alteration (CIA) expressed as the molar volumes of $[\text{Al}_2\text{O}_3 / (\text{Al}_2\text{O}_3 + \text{CaO}^* + \text{Na}_2\text{O} + \text{K}_2\text{O})] \times 100$, where CaO^* represents the CaO only from the silicate fraction (Nesbitt and Young, 1982, 1989) can be used as a tool for paleoweathering reconstructions (Fedo et al., 1997; Yan et al., 2010). As the samples contain some carbonate, as an approximation, the CaO^* is assumed to be equivalent to Na_2O (McLennan, 1993). To avoid errors derived from the unknown CaO content of the silicate fraction, the CPA (chemical proxy of alteration) after Buggele et al., 2011 (or CIW' - chemical index of weathering after Cullers, 2000) is additionally used: $\text{CPA} = 100 \times \text{Al}_2\text{O}_3 / (\text{Al}_2\text{O}_3 + \text{Na}_2\text{O})$.

Cr/Ni - and $(\text{Cr}/\text{V})/(\text{Y}/\text{Ni})$ -ratios (Garver et al., 1996, and McLennan et al., 1993) are used to indicate ultramafic detritus (ophiolitic input) in provenance studies.

3.4 BULK CARBON AND OXYGEN ISOTOPE CONTENTS

Stable isotope ratios of carbon and oxygen from 33 samples were analyzed from carbonate bulk (0.1 to 0.3 mg of untreated sample) with a mass spectrometer (on-line preparation using a Gasbench II interfaced to a ThermoFinnigan CF-IRMS) at the University of Innsbruck using the classical phosphoric reaction. The calibration was performed against VPDB with an in-house marble standard standardized against the international reference standard NBS 19. An analytical error (1 s.d.) of 0.06 respectively 0.08 permil for $\delta^{13}\text{C}$ and $\delta^{18}\text{O}$ based on the long-term performance of quality assurance material is denoted. The results are given in the usual delta notation (for details see Spötl and Vennemann, 2003).

The carbon and oxygen isotopy in carbonates basically depends on the isotopic composition of the water (respectively salinity) from which the carbonate precipitates and to some degree on temperature (Hudson, 1977). Non-marine carbonates are characterised by distinct lower $\delta^{13}\text{C}$ and $\delta^{18}\text{O}$ -values than marine carbonates – that means that they are enriched in the lighter isotopes. Therefore, carbon isotopes are widely used in combination with oxygen isotopy to interpret the genesis and facies (paleoenvironment, paleosalinity, thermometry, etc.) of sediments (Clayton and Degens, 1959; Hudson, 1977; Veizer, 1983; Talbot, 1990, Reinhardt et al., 2003). The statistic evaluation and analysis of the geochemical and isotopic data were done using the software package IBM SPSS Statistics 19.

3.6 MACERAL ANALYSIS OF COAL PARTICLES

One coal and four clay samples containing coaly particles (M1a, M5, M8A, M14, M17; see Fig. 3 for stratigraphic position) were investigated for maceral composition. Maceral analysis was performed by a single-scan method (Taylor et al., 1998) with a Leica MPV microscope using reflected white and fluorescent light. A maximum of 300 points was counted and the results are given in Online Appendix A. Vitrinite and inertinite macerals were classified according to the nomenclature proposed by ICCP (1998) and ICCP (2001). Vitrinite reflectance of samples was determined following established procedures (Taylor et al., 1998).

3.7 PALYNOLogy

Sample preparation for (terrestrial) palynomorphs followed standard procedures: The samples were crushed with a mortar and pestle, and the resultant rock powder treated with standard wet chemical processes using HCl and HF. In order to retain palynomorphs smaller than 10μ the organic extract was not sieved. Instead it was acetolyzed and mixed with glycerine and stored in small glass bottles. For examination under the LM, a drop of well-mixed extract was evenly distributed on a glass slide. For each sample 12 slides were carefully screened to yield both common and accessorial taxa, which occur in small numbers or only as single specimen. For LM photography (Nikon Coolpix) the investigated pollen grains were transferred via glycerine onto a glass slide. For further examination under the SEM (Jeol 6400 and FEI Inspect 500), the pollen grains were moved to a SEM stub, carefully washed with 100% alcohol to remove the glycerine and sputter coated

with gold. Stubs are stored in the Department of Palaeontology, University of Vienna.

3.8 CALCAREOUS NANNOFOSSILS

Fourty-seven samples of fine-grained sediments were studied using calcareous nannofossil content, applying standard smear slide techniques (e.g., Burnett, 1998). Samples were examined under the light microscope (1000x magnification) for judging the presence and estimating relative abundance of nannofossils (nannofossil specimen per field of view (pfv), using an arbitrary numerical scale by dividing the number of specimens by the number of field(s) of view, i.e. 1 specimen per 5 fields of views gives $1/5 = 0.2$ pfv). Additional 22 nannofossil samples were taken from the successions below and above the trench for biostratigraphic evaluation.

4. RESULTS

4.1 LITHOSTRATIGRAPHY

The sediments in the trench are overturned due to folding with an average orientation of 346/24 of the bedding surfaces (Figs. 4A, 5). Only few brittle faults have been observed in the trench (Fig. 4B). They show only small displacements and probably accommodate rheological differences of the diverse bed lithologies. Additionally competent beds within less competent sediments in several examples develop pronounced boudinage structures, which certainly influence the reconstruction of bed thicknesses.

The excavated section exposes only a part of the Lower Campanian Grünbach Formation. Neither the contacts to the Maiersdorf Formation below, nor to the Piesting Formation above have been unearthed (Fig. 2). Figure 1 shows the trench location in the middle part of the Grünbach Formation. The horizontal distance from the respective endpoints to the underlying Maiersdorf Formation and the overlying Piesting Formation is in both directions approximately equal to the trench length (141 m). In the trench almost 45 m lithostratigraphy has been recorded and thus similar thicknesses might be expected for the unexposed sediments of the Grünbach Formation in the hanging wall and foot wall of the trench.

4.2 SEDIMENTOLOGY

The exposed Gosau sediments comprise clay, marl, siltstone, sandstone with rare conglomerate and coal (Figs. 3, 5, 6; see Summesberger et al., 2002). Seven thin, black, organic rich beds have been documented. According to the maceral analyses, however, only one real coal horizon (M17) does exist whereas the others comprise mainly allochthonous accumulation of coal (see Fig. 3).

The exposed section starts with clay (M92, M90), intercalated with a sandstone bed (Fig. 3). Above follows a thin horizon with allochthonous accumulation of coal (M88), directly overlain by a conspicuous brownish limestone which is extremely rich in the green algae *Munieria* sp., indicating fresh-water to brackish environments (Schlagintweit and Wagreich, 1992; Rákosi and

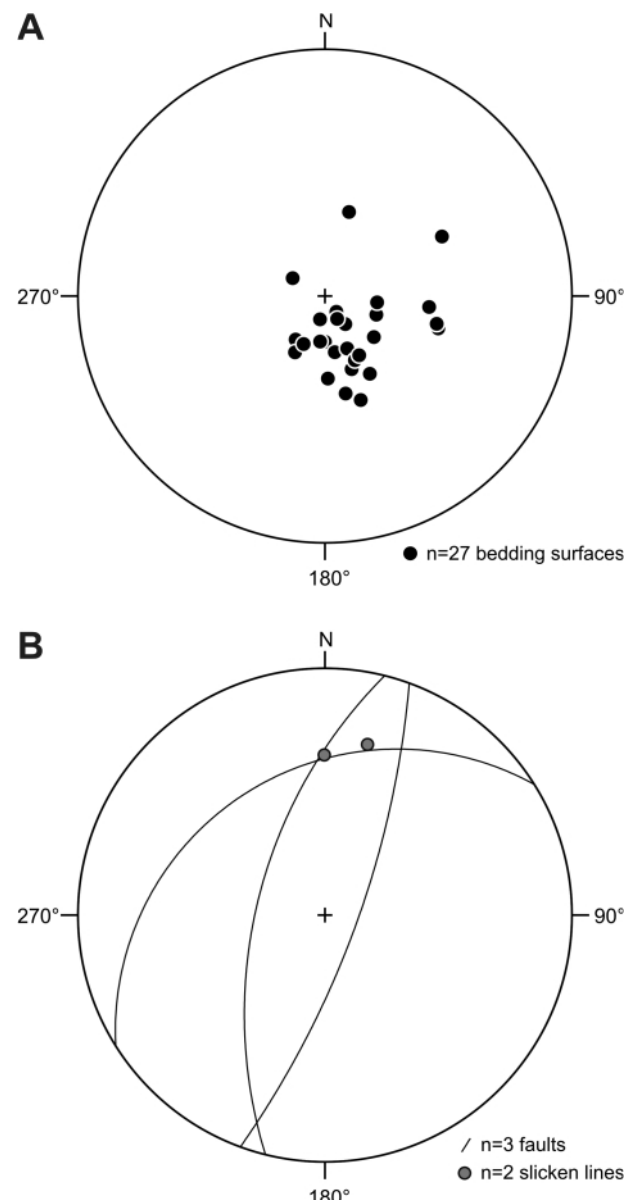


FIGURE 4: A. Orientation of bedding surfaces exposed in the investigated trench. The bedding surfaces are overturned due to folding with an average orientation of 346/24. B. Fault surfaces and slicken lines exposed in the investigated trench. Faults have been documented at trench running meters 61m, 70.5m and 128.2m. The displacements are generally small and probably result from competence contrasts of different beds during folding. Both plots equal angle projection, lower hemisphere.

Barbacka, 1999/2000) thin-section in Figure 6A). This noticeable limestone additionally contains shell fragments and is succeeded by a thick argillaceous marl layer with marine ostracods, foraminifera and several solitary corals (*Cyclolites* sp., Hannes Loeser, pers. comm. 2010) (Fig. 5B) in life position at its base, confirming the overturned orientation of the beds in the trench.

Above, about 5 m thick alternations of relatively thin marl and sandstone beds with some nannofossils documented in the upper part are present. One of these beds (M81) contains shell fragments and two thin horizons with allochthonous accumulations of coal (M74, M67). In general, the fine grained

beds within the first 10 m show higher carbonate contents compared to similar sediments higher up in the section.

The next 20 m (M65-M43) are dominated by relatively thick sandstone beds interrupted by beds of relatively thick clay and calcareous clays. Brownish colours dominate in both, fine-grained and sand-sized sediments, changing to greenish colours between 25-30 m of the section. Nannofossils in this interval are restricted to the lowermost beds and only one very thin horizon with allochthonous accumulation of coal has been observed. The marl bed M57 contains two fragments of abraded miliolid foraminifera.

Then 2 m of clay (M42-M41) are followed by a some 5 meters thick alternation of relatively thin beds of clay, calcareous clay and sandstone, including two polymict conglomerate layers (M38, M39) (Fig. 3). The fine-grained beds in this part change from brownish to yellowish colours to gradually darker gray.

The final 8 m of the section are dominated by medium to dark gray carbonaceous clay and calcareous clay and three beds with allochthonous accumulations of coal. One of these has a thickness of 25 cm and counts as real coal as indicated by organic petrology (M17, see Online Appendix A). This interval contains several layers with nannofossils and two horizons with shell fragments divided by non-marine clays (Fig. 3).

4.3 CALCIUM CARBONATE AND TOTAL ORGANIC CARBON CONTENT

The calcium carbonate contents of the samples from the trench range from 0 (coaly samples) to 78% with a mean of 22% (Fig. 7, Online Appendix B).

High amounts of TOC correlate with coal and layers with allochthonous accumulations of coal (between 21 and 34% for the samples M1, M5, M67, M74 and M88) up to 52.8% (M17). Moderate TOC contents up to 12% can be seen for many samples (Fig. 7). Shales and marls without visible plant fragments or coal seams have typically TOC contents between 0.05 and 12.05. High sulphur contents of coals and layers with allochthonous accumulation of coal from the trench (e.g. M17, M1, M5, M7) may indicate brackish-marine influence. According to Sachsenhofer (1987 and personal communication 2010) the coals of the eastern part (Piesting, Maiersdorf) of the syncline generally show higher sulphur contents than those of the western part (Grünbach) and are therefore regarded as reworked into the marine intervals (Sachsenhofer, personal communication 2010).

4.4 WHOLE-ROCK GEOCHEMISTRY

Results are summarized in Figure 7 and listed in Online Ap-

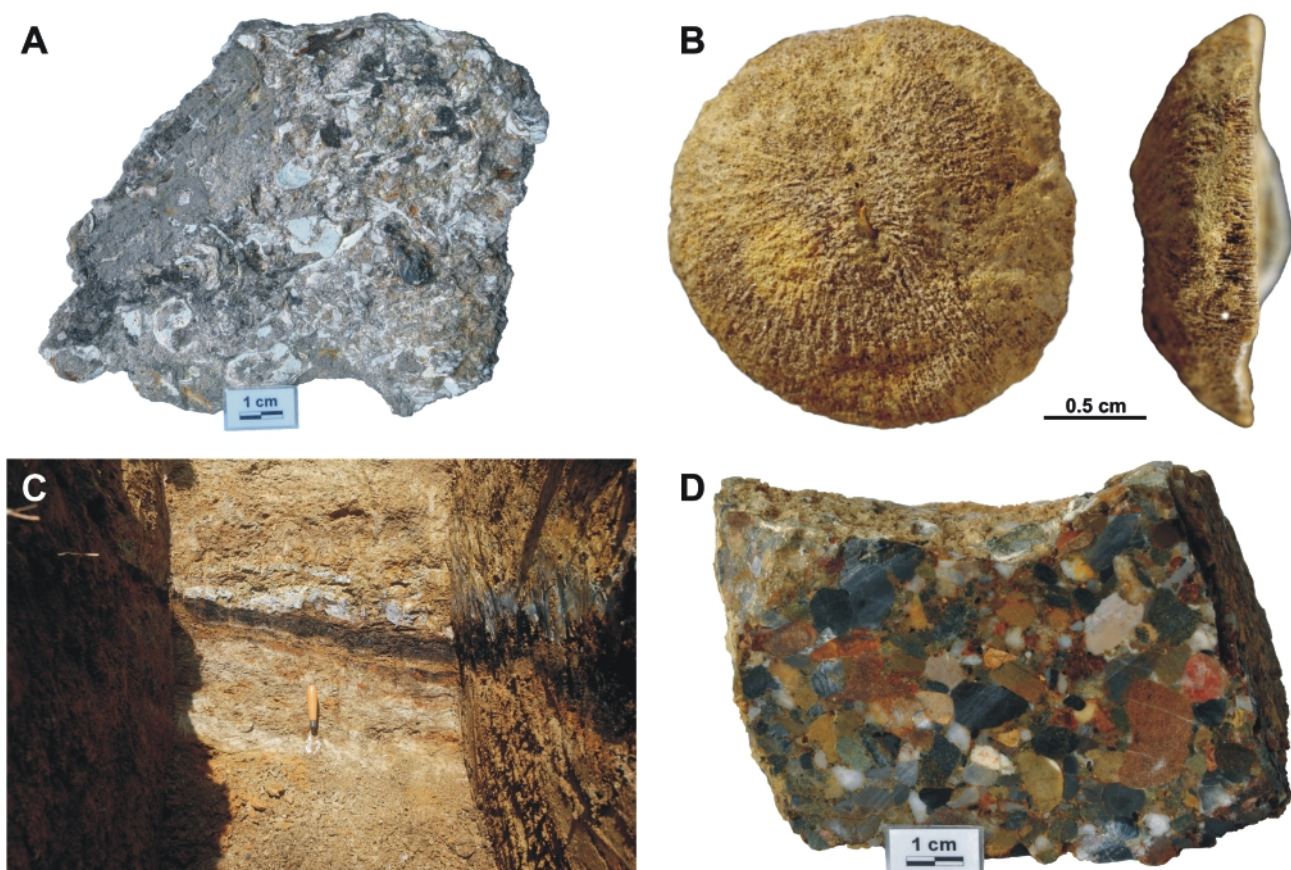


FIGURE 5: Examples of lithologies documented in the trench (see Figure 3 for samples location). A. Bedding surface of the limestone (M86) with shell fragments. B. Very well preserved solitary coral *Cyclolites* sp. (M85) from directly above the coal layer of M88. C. Typical trench exposure showing the interval at the coal bearing bed M67 and the fine grained beds immediately above and below dipping in overturned orientation at c. 25 degrees towards the NNW. D. Polymict conglomerate (M38) dominated by carbonate clasts from the Northern Calcareous Alps, interpreted to correlate with Dreistetten conglomerate further to the east of the syncline.

pendix B. Samples are generally characterised by relatively high boron concentrations (up to 272 ppm) with a mean of 149 ppm (st.dev.= 41.7) and show a trend from lower to higher values from bottom to top. Only 4 samples have typical non-marine values (between 62 and 89 ppm) which correspond exactly to the coaly horizons (M60, M67, M74 and M88) in the lower part of the profile. Samples from coaly layers in the upper part show shifts to lower boron contents but typical non-marine values (at least under 100 ppm) are missing. In the lowermost 10 meters the boron values fluctuate strongly from layer to layer (between 62 and 190 ppm). The middle section between 10 and 35 meters is relatively uniform with boron contents at around 140 ppm. The uppermost 10 meters of the profile are characterised by higher mean values of around 180 ppm and a higher degree of variation including the maximum value of 272 ppm for sample M9B (Fig. 7).

The B/Al* curve shows strong similarities to the boron curve with a mean ratio of 206 (st.dev.= 210.9). While in the lower part of the profile shifts to lower ratios within coaly beds are characteristic, the coaly samples at the top show an extremely high ratio (up to more than 1365), highlighting geochemical differences of the coals respectively coaly sediments in the lower and upper part (Fig. 7).

Th/U ratios alternate between 0.35 and 5.00 (mean=3.19) at which uranium is relative to thorium enriched in mud and organic matter resulting in low Th/U ratios for coaly samples. The lowest ratio of 0.35 (and the highest TOC of 52.8%) is represented by the “real” coal sample M-17 (Fig. 7).

The CIA values are all quite uniform and range between 73.4 and 83.0 with a mean of 76.3 (Figs. 7, 8). The CPA values also have a relatively small range between 92.7 and 98.1 and show similar trends compared to the CIA, which results in a strong positive correlation ($r=0.866$) (Fig. 7).

Chromium and nickel contents are rather low: chromium concentrations are not higher than 155 ppm (mean=100.8), nickel values range between 5 and 97 ppm with a mean of 53.0 (Fig. 9A).

Cr/V and Y/Ni ratios are uniform and low, between 0.21 and 0.97 (mean=0.68) respectively between 0.29 and 4.73 (mean=0.65) (Fig. 9B).

The discriminant function plots (after Roser and Korsch, 1988) do not indicate clear results (Fig. 10). The samples cluster around the intersection of the source end members “mafic” (coaly samples are related to this section), “intermediate”, “felsic” and “quartzose”.

4.5 BULK CARBON AND OXYGEN ISOTOPE CONTENTS

$\delta^{13}\text{C}$ ratios fluctuate between -9.3 and 0.3 ‰ VPDB and with a mean of -5.2 ‰ they are comparatively low. Similar to the boron concentrations a lowermost part with highly variable ratios (most of the extreme low values at around -8 ‰ as well as the maximum value is within these lower 11 meters) and a relatively constant middle interval between 11 and 35 meters (mean around -6.7 ‰) can be observed. At around 33 m the

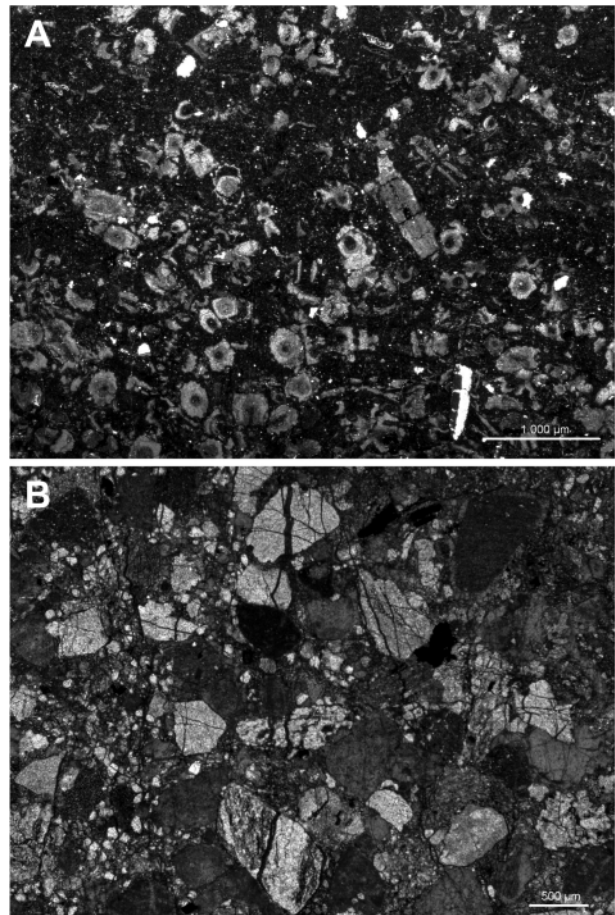


FIGURE 6: Thin-sections. A. Limestone (M86) with abundant alga *Muneria* sp. B. Medium to coarse grained sandstone (M15) dominated by subangular quartz and rounded carbonate clasts.

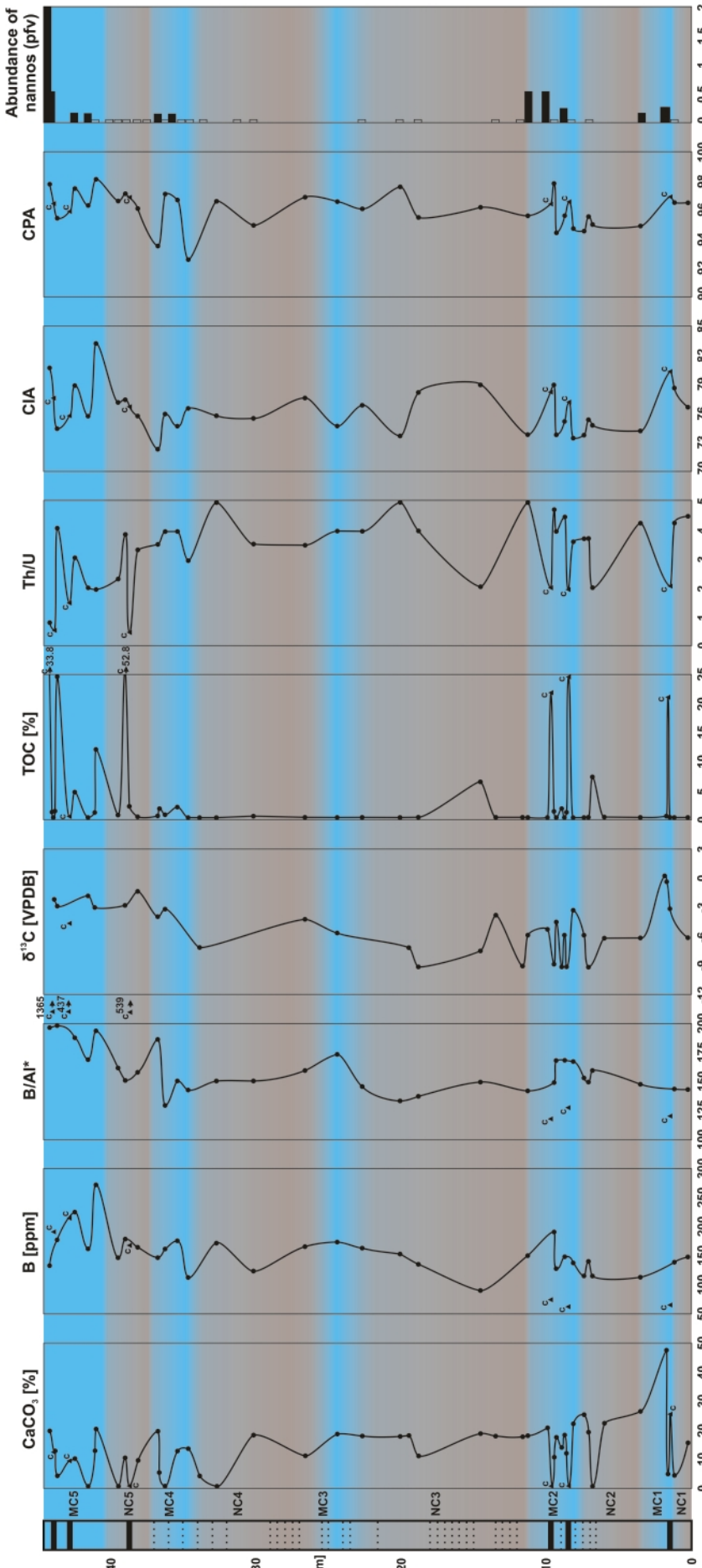
$\delta^{13}\text{C}$ isotopy increases to mean values of about -3 ‰ with the highest value up to -1.42 ‰ of this top section between 35 and 44.5 meters (Fig. 7).

$\delta^{18}\text{O}$ ratios are also relatively low and fluctuate between -10.0 and -5.2 ‰ VPDB. Generally $\delta^{18}\text{O}$ values correlate well with $\delta^{13}\text{C}$ ratios with relatively low values typically between -7 and -9 ‰ VPDB in the lower and middle part of the section and higher values between -6 and -5 ‰ VPDB at the top (from around 35 to 44.5 meters).

4.6 MACERAL ANALYSIS OF COAL PARTICLES

Most of the investigated samples comprise allochthonous accumulation of coals (e.g. Glasspool, 2003), i.e. pieces of vitrinite, gelified wood fragments, and cutinite in clay (e.g. M1A, M5, M8A, M14). Wood structures are faintly indicated by fluorescence. Samples are interpreted as remnants of driftwood or roots in clay. Sample M8A additionally shows liptinite (resinite or flourinite) that appears in otherwise structureless humous masses. The only real coal sample (M17: vitrinite 86 vol.%, liptinite: 11 vol.%, Inertinite: 3 %) also contains mainly detrital gelified coal, remnants of leaves (cutinite and phyllohuminitite ca. 10 vol.%); additionally spores, inertinite and semiinertinite, and a high pyrite content (Online Appendix A).

The values of vitrinite reflexion 0.50 und 0.52%Rr are slightly



lower than values from Grünbach coal samples measured by Sachsenhofer (1987). The lower values may result from weathering (Ivanova and Zaitseva, 2006) of the near surface samples of the trench compared to fresh samples from underground mining used by Sachsenhofer (1987).

4.7 PALYNOLOGY

First pollen data of the Grünbach Formation have been provided by Draxler (1997). In all our analyzed samples the palynofloras are very poor and partly badly preserved. All the members of the morphogenera of the pollen are characteristic for the time span between late Santonian to Maastrichtian. The characters of the “Normapolles” (extremely thick walls, very protruding aperture areas) are typical for this period (Scarry, 1986).

The organic facies is generally composed of semi-opaque matter (such as darkened, gelified wood fragments) few fungal spores and hyphen, and very few cuticular, membranous material. The cavities of many pollen grains are filled with autogenic pyrite crystals.

In the pollen and spores assemblages the most thick-walled and resistant taxa have been preserved. Spores are represented by *Laevigisporites* and *Concavisporites* types (unknown botanical affiliation), *Cicaticosisporites* and *Cingulatisporites* types (Schizaeales, *Aneima* and *Lygodium*, respectively) and livermoss spores. Angiosperm pollen are generally presented by the “Norma-

FIGURE 7: Simplified profile of the Maiersdorf-trench (black layers represent coal or allochthonous coal layers) with selected geochemical parameters CaCO₃, B, B/Al*, δ¹³C, TOC, Th/U, CIA and CPA. Black dots symbolize pelitic samples, black triangle and “c” stand for coals or allochthonous coal. The trendline of the parameters B, B/Al* and δ¹³C does not include coal and allochthonous coal. Semi-quantitative values for the abundance of calcareous Cretaceous nannofossils (pfv; see text) are added: blank bars symbolize blank nannofossil samples, black bars are samples including nannofossils. Five non-marine (NC1 to NC5) to marine cycles (MC1 to MC5) interpreted from geochemical and supported by fossils are highlighted in brown and blue.

"polles" group: extremely variable/diverse *Slowakipollis*, *Krutzschipollis*, cf. *Longanulipollis*, cf. *Hungaropollis*, *Trudopollis*, *Oculipollis* and *Nudopollis* species (many of them with strong Juglandalean affinities seen in the exine pattern), *Complexiopollis* spp., (Myricaceae affinities), *Vacuopollis*, etc. All the different existing species (to some extant genera, have been formerly defined under the lightmicroscopy investigation alone) should be handled with care, because of the extreme variability of these ancient genera (compare Scarby, 1986).

Other angiosperm pollen types are even rarer: Monosulcates (not yet identified taxa), *Minorpollis* (Juglandalean), *Myrtacedites* (true Myrtaceae), *Clavatipollenites* spp. (Chloranthaceae), Platanaceae, tricolporate hamamelidaceous type, tricolporate not affiliated types and *Spinizonocolpites* (*Nypa* palm).

The occurrences of the megathermal Schizaeles ferns, *Normapollis*, Myrtaceae, Chloranthaceae and *Nypa* (tropical mangrove palm, *Spinizonocolpites*) evidence very warm and humid depositional conditions, somewhere close the coastline. The observation of *Nypa* pollen in trench samples represents the northernmost occurrence so far. The previously northernmost finding of *Nypa* pollen has been from Campanian/Maastrichtian drill cores of northwestern Egypt (Schrank and Ibrahim, 1995).

4.8 NANNOFOSSILS

Nannofossils recorded in the trench section do not include marker species that would allow a biostratigraphic zonation. Only a few long-ranging taxa like *Watznaueria barnesae*, *Zeughrabdota* spp., *Rhagosdiscus* spp., *Prediscosphaera* spp. were found in a few samples. This corroborates the overall marginal marine to non-marine character of sedimentation. However, nannofossil abundance data, though always rare to very rare if not absent at all, can be used to infer possible marine or nonmarine depositional environments and to compare this data with geochemical proxies (Figs. 3, 7).

5. DISCUSSION

5.1. TRENCH LITHOSTRATIGRAPHIC POSITION WITHIN THE GRÜNBACH FORMATION

Due to the fact that the trench is located entirely within the Grünbach Formation the exact position in meters above the base of the formation and the correlation with published sections (Plöchinger, 1961) remains ambiguous. A small depression with a tree just south from the eastern end of the trench probably represents the location of the former ventilation shaft indicated in the mining plan of the Neuhoffnungs Stollen (gallery). Based on the location of the gallery mouth and the ventilation shaft in the ALS digital elevation data (Fig. 1) and the

Student's t-test							
Variable	Interpreted salinity	N	Mean	St. Dev.	T	Significance	
B [ppm]	non-marine	15	139.0	25.26	-2.232	0.034	
	marine	16	165.8	39.45			
B/Al*	non-marine	15	149.4	8.57	-3.189	0.005	
	marine	16	167.2	20.48			
$\delta^{13}\text{C}$ [VPDB]	non-marine	12	-6.34	2.532	-1.924	0.064	
	marine	20	-4.51	2.644			
$\delta^{18}\text{O}$ [VPDB]	non-marine	12	-7.52	1.209	-1.383	0.177	
	marine	20	-6.90	1.244			

TABLE 1: Results of the Student's t-test calculation for the variables B, B/Al*, $\delta^{13}\text{C}$ and $\delta^{18}\text{O}$ with number of samples (N), mean, standard deviation, T-value (T) and significance for the test (α).

orientation as well as scale of the mining plan, the sediments of the trench can approximately be correlated to the geological documentation of the gallery. Based on this correlation the sandstone dominated interval with some conglomerate beds between 12 to 33 m of the trench section (Fig. 3) might be correlated with the Dreistetten Conglomerate of Plöchinger (1961) (Fig. 2).

5.2 PALEOENVIRONMENT RECONSTRUCTION BASED ON GEOCHEMISTRY

Considering all geochemical parameters (especially B contents, B/Al* and stable carbon and oxygen isotopic ratios) in combination with calcareous nannofossil abundances and lithofacies characteristics, five large-scale non-marine (NC) to marine facies cycles (MC) can be interpreted. The geochemical characteristics of coals differ significantly from pelitic sediments, and therefore some geochemical features like the TOC or B/Al* ratio can vary drastically in sediments associated with coals. We therefore did not include coaly layers in our general

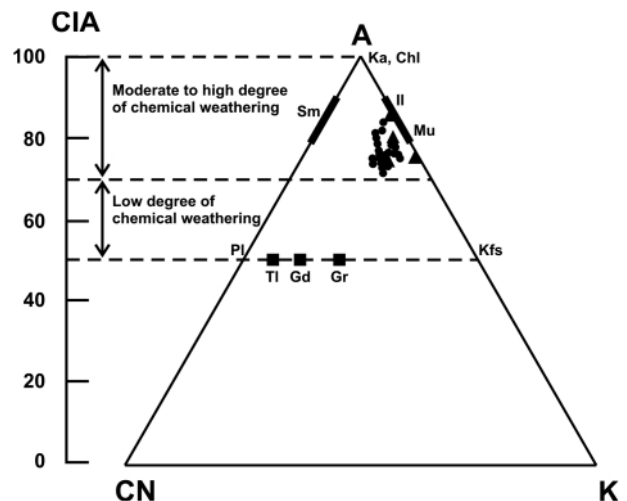


FIGURE 8: A-CN-K ($\text{Al}_2\text{O}_3\text{-CaO}^*+\text{Na}_2\text{O}\text{-K}_2\text{O}$) ternary diagram of samples from Maiersdorf-trench (dots symbolize pelitic samples, triangles coals and coaly samples) and associated chemical index of alteration (CIA) after Nesbitt and Young, 1982. Squares and bars symbolize the average composition of tonalite (Tl), granodiorite (Gd) and granite (Gr) as well as kaolinite (Ka), chlorite (Chl), smectite (Sm), illite (II), muscovite (Mu), plagioclase (PI) and K-feldspar (Kfs).

geochemical paleoenvironment interpretations, although values are included into the tables (Online Appendix B) and figures (marked with c).

The stratigraphically lowermost cycle NC1 (0-1.4 m) is characterised by moderate B and B/Al* concentrations as well as low $\delta^{13}\text{C}$ and $\delta^{18}\text{O}$ ratios. Within this section, no nannofossils could be found which corroborate a non-marine environment. Geochemical and nannofossil data suggest therefore a clearly non-marine interval (Fig. 7, Online Appendix B).

Above a characteristic coaly layer, high $\delta^{13}\text{C}$ (up to -0.57 ‰ VPDP) and $\delta^{18}\text{O}$ ratios in combination with the rare presence of nannofossils and marine macrofossils (corals, gastropods and bivalves) give evidence for a period of predominantly marine sedimentation (MC1; 1.4-2.8 m of the section). Boron and boron normalized with aluminum, however, show shifts to lower values which do not correspond to the overall interpreted facies trend (Online Appendix B, Fig. 7).

NC2 (2.8-8.0m) shows relatively low B and B/Al* values and a distinct shift to low $\delta^{13}\text{C}$ and $\delta^{18}\text{O}$ ratios. Additionally, within this interval no nannofossils could be found (Online Appendix B, Fig. 7).

The interval between 8.0-11.5 m is characterized by moderate to high B values and B/Al* ratios as well as relatively low mean $\delta^{13}\text{C}$ and $\delta^{18}\text{O}$ ratios below -6.50 ‰ VPDB. The two horizons with coaly sediments are geochemically distinct within this interval characterized by low B values below 74 ppm. Nevertheless, high nannofossil abundances suggest a marine depositional environment (MC2) throughout this interval although the chemical evidence for marine sedimentation is ambiguous (Online Appendix B, Fig. 7).

After that, a long period with a lack of nannofossils from 11.5 to 23.9 m is present (NC3). The boron and aluminium normalized values are relatively low and uniform, stable isotope ratios are characteristically low and regarded typical for non-marine environments (Fig. 7, Online Appendix B).

Small positive shifts of boron and carbon isotope ratios as

well as a lithological change from yellow to brown mud and sandstones to grey and greenish mud and sandstones may indicate a brackish to marine interval (MC3, 23.9-27.0 m). For this interval, however, no supportive nannofossil or macrofossil data are available to corroborate the brackish-marine interpretation (Online Appendix B, Fig. 7).

NC4 (27.0-34.7m) is very similar to NC3 in lithology (sandstones are dominant) and geochemistry with low B/Al* and carbon isotope ratios as well as low to moderate boron values (Online Appendix B, Fig. 7).

Rare nannofossils have been found in MC4 (34.7-37.1 m); additionally positive shifts especially in the stable carbon isotope and B/Al* ratios can be observed within this section and give evidence for a marine environment.

A lack of nannofossils, dark marls, and a 25 cm coal layer (M-17) characterize NC5 (37.1-40.5 m). Although there is a negative shift of boron concentrations and ratios (except the extremely high value for the coal sample), mean values of B, B/Al* and $\delta^{13}\text{C}$ stay overall high and do not fully support the non-marine facies interpretation (Fig. 7) but, compared to the overlying MC5 (40.5-44.7m), values are more "non-marine", i.e. lower in boron and carbon isotopes as a positive shift of boron values and carbon isotopes (mean=-3.0 ‰) is characteristic for the top section MC5. This interval is additionally characterized by a higher amount of nannofossils (pfv up to 2) and a marine macrofossil fauna of bivalves and gastropods. The coaly mud sample M1B has an extremely high B/Al* ratio of 1365 (Online Appendix B, Fig. 7).

Pearson correlation indices of the variables B, B/Al*, $\delta^{13}\text{C}$ and $\delta^{18}\text{O}$ (Fig. 11) all show positive relations of different significances and illustrate the geochemical coherence of these variables. A positive correlation of $r=0.394$ between B and B/Al* (excluding coaly samples) as well as distinct discrimination of samples interpreted as marine and non-marine, i.e. higher B and B/Al* values for marine samples, are significant. Further, a significant positive correlation for $\delta^{13}\text{C}$ and $\delta^{18}\text{O}$ can be ob-

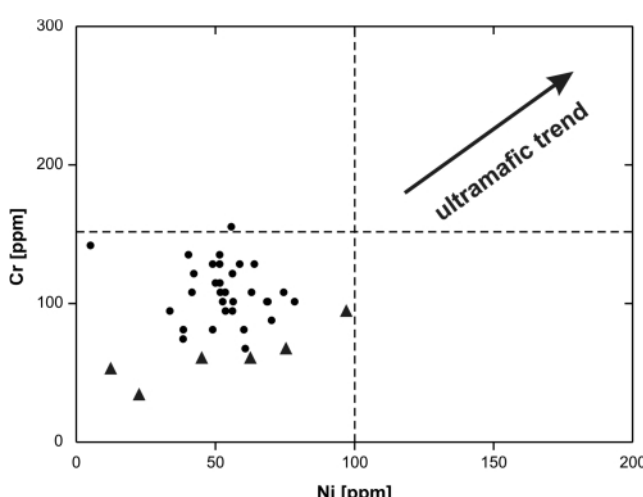
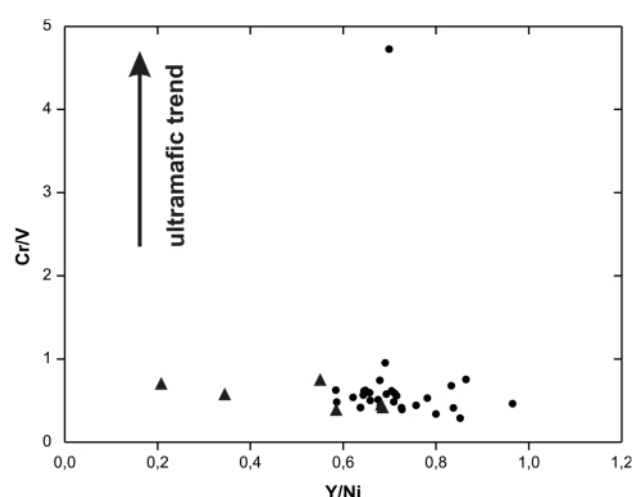


FIGURE 9: Geochemical discrimination plots based on ultramafic/ophiolitic detrital trends. A. Discrimination using Ni and Cr (after Garver et al., 1996) The dashed lines mark the limits enriched Ni (100ppm) and Cr (150ppm). B. Discrimination using Y/Ni and Cr/V (after McLennan et al., 1993). Dots symbolize pelitic samples, triangles coal and allochthonous coal.



served (Fig. 11) but the discrimination effect between marine and non-marine samples is not so distinct. Although this correlation indicates significant diagenetic overprint of the primary isotope signal the isotope data still can be used for the differentiation between marine and non-marine environments as indicated by the statistical significance tests (see Table 1). In contrast, relatively weak positive correlations are characteristic for B and B/Al* in combination with $\delta^{13}\text{C}$ (Fig. 11e,f).

Student's t-test analysis of B, B/Al*, $\delta^{13}\text{C}$ and $\delta^{18}\text{O}$ were calculated excluding all coaly samples. This comparative method of means and standard deviations demonstrates that boron concentrations are significantly lower in non-marine interpreted intervals (Table 1).

The mean value of the B/Al* ratio is also lower for samples interpreted as non-marine compared to the mean of the marine interpreted sample group. Due to the fact that the variances of the two groups are different for the B/Al*, which was proven by the Levene test, the Student's t-test for heterogeneous variances was used. With a high significance of $\alpha=0.005$ marine and non-marine B/Al* ratios are distinctively different (Table 1).

Stable isotope ratios of $\delta^{13}\text{C}$ and $\delta^{18}\text{O}$ have more negative values within non-marine interpreted intervals relative to marine intervals. While for the $\delta^{13}\text{C}$ values the significance is just below the limit, the $\delta^{18}\text{O}$ ratios do not differ statistically significantly from marine and non-marine samples (Table 1).

The chemical index of alteration (CIA) values show in general high values between 73 and 85, indicating a significant trend of increasing chemical weathering during the time of deposition of the Grünbach Formation. This is in accordance with the moderate greenhouse climate suggested for the Campanian (e.g. Jenkyns, 2003) and supported by palynology data indicating warm and humid conditions. In detail, there are slight fluctuations recorded from more moderate to higher chemical weathering, which correlate with most of the marine intervals identified by nannofossil and boron content. This may be interpreted as a result of a more pronounced chemical weathering during transgressive to sea level highstand periods.

The TOC/S ratios are fluctuating quite drastic and do not show any systematic variation in regard to identified marine or non-marine intervals and, therefore, doesn't qualify as a reliable means to identify depositional environments in our data.

5.3 SEDIMENTARY ENVIRONMENTS AND COAL FORMATION

In general, a non-marine to shallow marine environment of deposition is supposed for the Grünbach Formation (Plöchinger, 1961; Summesberger et al., 2002). High sulphur contents of some of the coals indicate a brackish-marine influence also on coal deposition (Sachsenhofer, 1987, personal communication 2010; see also Schulz and Fuchs, 1991) and, in general, a flood plain to marginal marine environment was inferred for this formation (Summesberger et al., 2002). Our results indicate the presence of large-scale non-marine to brackish-marine cycles and marine environments for at least parts of the Grünbach Formation in contrast to previous, solely non-marine-brackish interpretations (Plöchinger, 1961; Summesberger et al., 2002).

An alluvial fan to fan-delta environment is suggested as the most proximal non-marine facies, and is present as conglomerate layers and conglomerate-sandstone bodies such as the prominent Dreistetten conglomerate, which has a higher thickness to the east of the trench site. Sandstone and shale successions with coals and/or coaly shale layers are interpreted as fluvial-lacustrine to coastal plain sediments in a humid climate with the presence of swamps and mires. Rapid transgressions, as evidenced by fast transitions from coaly layers to fully marine, coral-bearing marls such as at the boundary of cycle NC1-MC1 (Figs 3, 7), raised the groundwater level and fostered coal formation. Marginal marine environments, representing the maximum flooding of transgressive cycles, comprise either sandy fan delta sediments or, as evidenced from the trench section, typically fine-grained marly inner shelf bioturbated pelites with some macrofauna like corals and molluscs, to fine-grained lagoonal deposits with marls and rare

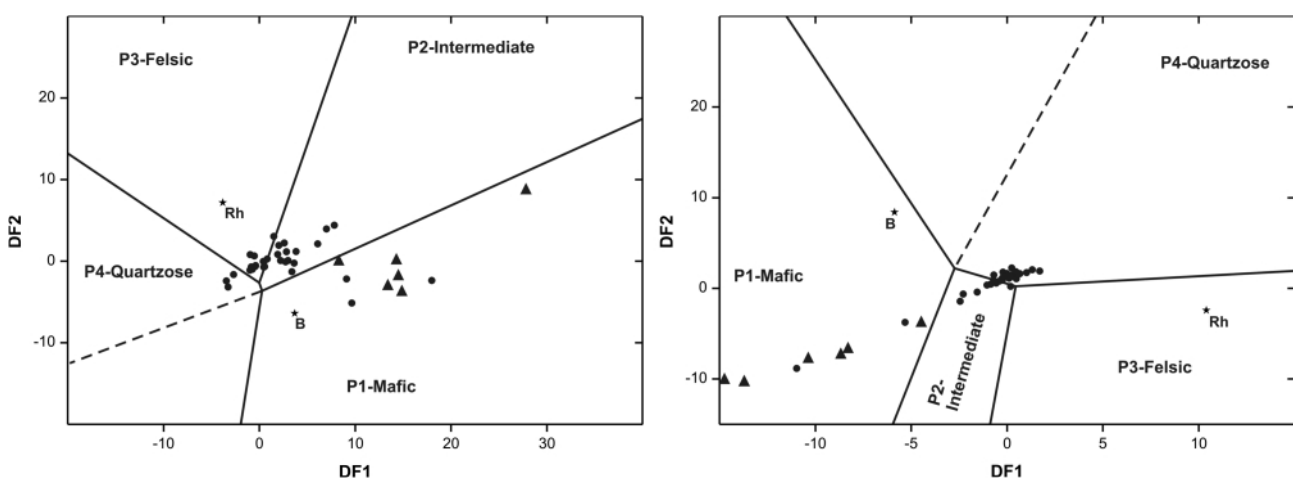


FIGURE 10: Discrimination plot of discriminant function 1 (DF1) and 2 (DF2) showing 4 main provenance groups: P1-mafic, P2-intermediate, P3-felsic and P4-quartzose (after Roser and Korsch, 1988). Dots symbolize pelitic samples, triangles coals and coaly samples. An average basaltic (B) and rhyolitic (Rh) composition is additionally plotted.

miliolid foraminifera and marine ostracods. In-situ positions of corals, the lack of any coarser grained clasts or other fossil fragments argue against significant storm transportation.

5.4 PROVENANCE

Based on sandstone petrology and heavy mineral studies the provenance of Gosau Group sediments of the NCA shows a complex evolution including local, ultramafic ophiolitic and me-

tamorphic sources (e.g. Wagreich and Faupl, 1994). In general, the provenance evolution based on heavy minerals starts with local sources (mainly stable minerals like zircon and tourmaline together with apatite) with variable admixture of ophiolitic detritus (chrome spinel), followed by low- to high-grade metamorphic detritus (garnet, staurolite, chloritoid among other metamorphic minerals).

From the geochemical point of view an ultramafic/ophiolitic

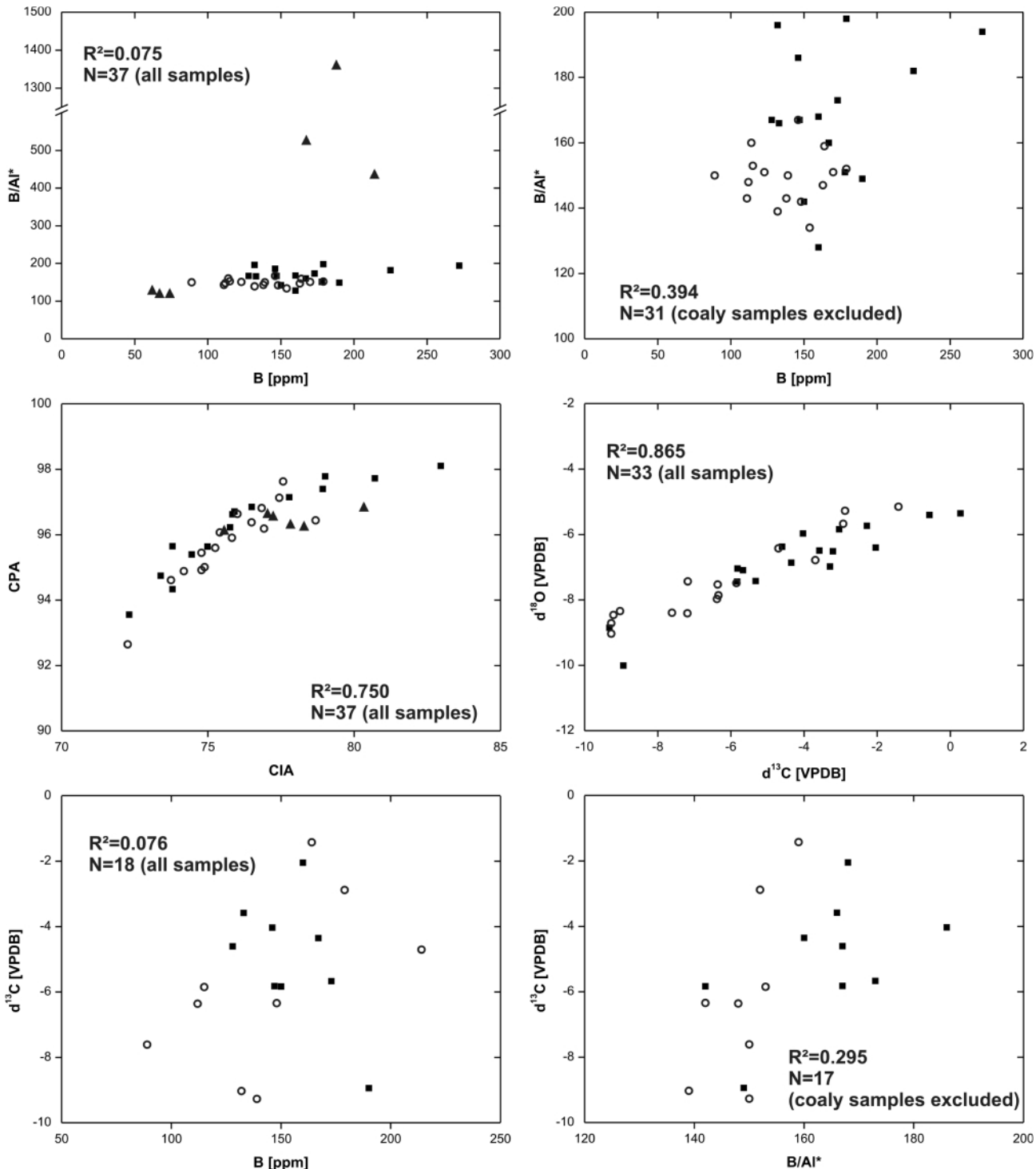


FIGURE 11: Geochemical discrimination plots of B and B/Al* (for all samples and without coaly samples M1b, M5, M17, M67, M74 and M88), CIA and CPA, $\delta^{13}\text{C}$ and $\delta^{18}\text{O}$ as well as B and $\delta^{13}\text{C}$ (for all samples and without coaly samples M5). Number of samples (N) and squared Pearson correlation index (R^2) is shown in the graphs. Black squares: marine; white circles: non-marine; black triangles: coals.

source cannot be proven. The chromium and nickel limits of 150 ppm respectively 100 ppm indicative of ultramafic sources according to Garver et al. (1996) are not exceeded. Furthermore, no enrichment of the Cr/V ratio relative to the Y/Ni ratio was observed in our data which would be characteristic for ophiolitic detritus (McLennan et al., 1993).

The discriminant function analysis using major elements (Röser and Korsch, 1988) achieves no clear results. The samples plot in all end members of sources and cluster around the intersections. A mixed provenance is most likely for this complex tectonic regime of the Gosau basin in the Early Campanian.

5.5 MARINE – NON-MARINE CYCLICITY

The interpretation of marine - non-marine cycles in the investigated section is mainly based on the occurrence of nannofossils as well as geochemical and isotopic proxies. Due to the rarity of fossils the recognition of cycles is challenging (compare with Herm, 1977; Sanders, 1998). Based on our data 5 large-scale marine – non-marine cycles are reconstructed, some of them associated with coal formation (Figs 3, 7). Generally, the marine cycles are dominated by argillaceous sediments, the terrestrial cycles by sandstone and in rare cases by conglomerate. Brackish-marine influence is also indicated by the high sulphur contents of several coal samples (see maceral analysis; compare Schulz and Fuchs, 1991).

The geochemical proxies for the lowermost 4 beds (NC1) indicate conclusively non-marine environments (Fig. 7), supported by the presence of the limnic/brackish calcareous algae *Muniera* sp. (Schlagintweit and Wagreich, 1992), overlain by marl with solitary corals in life position, evidencing an abrupt change to marine conditions of MC1 (Fig. 3).

NC2 is dominated by arenaceous beds whereas MC2 is dominated by calcareous mud and marl. Two thin beds with coal particles might indicate short term sea level fluctuations to terrestrial conditions, but the overall marine character is convincingly shown by abundant nannofossils (Fig. 3).

The 12 m thick terrestrial cycle NC3 is the thickest in the section and dominated by sandstone beds. Rare fragments of abraded foraminifera in marl of M57 are interpreted as reworked (question mark in Fig. 3) and could have resulted from coastal wind transport (e.g. Teller et al., 2000). The environmental interpretation of MC3 above is solely based on geochemical data (Fig. 7 and Online Appendix B).

Cycle NC4 is very similar to NC3 and contains one thin conglomerate bed (M38) overlain by MC4, dominated by bluishgrey clay with thin sandstone beds. The terrestrial cycle NC5 is quite rich in organic matter (Online Appendix B) and contains the only unambiguous coal seam (M17, Online Appendix A) in the excavated trench. The dominance of allochthonous coal is similar to the (slightly older) coal beds of the Brandenberg Gosau in Tyrol (Schulz and Fuchs, 1991). NC5 ends with a thin conglomerate bed (M10) (Fig. 3) and is followed by MC5, which is dominated by bluish-grey clay and thin beds with coal particles. Nannofossils documented in several samples and geochemical data indicate predominantly marine depositional environments.

The whole Grünbach Formation has an estimated thickness of about 135m at the trench site, with some 45m exposed by the trench, positioned in the middle part of the Grünbach Formation. Given a maximum time span of c. 7.5 Myr for the sedimentation of the Grünbach Formation (Early Campanian, 83.5 Ma for the top of the underlying Maiersdorf Formation, 76 Ma for the base of the overlying Piesting Formation based on Summesberger et al., 2002, using the timescale of Ogg et al., 2004) gives a mean cycle duration of several hundred kyr. Eustatic cycles recognized by Miller et al. (2005b) at the New Jersey Atlantic margin are one magnitude longer (1-5 Myr), although some shorter cycles are also recognized there (e.g. Mizintseva et al., 2009). Recently, 405 kyr climate cycles resulting in eustatic sea-level changes are increasingly recognized in the Late Cretaceous record (e.g. Gale et al., 2002; Locklair and Sageman, 2008; Voigt and Schönfeld, 2010), and thus may explain the terrestrial-marine cyclic record of the Grünbach Formation.

However, the position of the Grünbach Gosau basin at an active tectonic margin (e.g. Wagreich, 1993) may alternatively suggest tectonically induced relative sea-level changes as cause for "cyclic" rapid marine transgressions and subsequent fill of the generated accommodation space, maybe superposed on eustatic cycles.

The type of cycle control cannot be separated yet with confidence between tectonic and (eustatic) sea-level changes governed by climate. The uniform provenance evolution as suggested by the geochemical and heavy mineral data of our study may point to minor tectonic movements during the deposition of the Grünbach Formation. Also the total thickness of sediment which accumulated during this time span (c. 135 m) is rather low as compared to clearly tectonically driven sedimentation elsewhere in the NCA during this time interval, e.g. 1000 m of Upper Turonian to Santonian sediments in the Gosau pull-apart basin (Wagreich and Decker, 2001). The mean sediment accumulation rate of 1.8 cm/kyr in the investigated Grünbach Formation is rather low compared with > 10 cm/kyr in the Gosau pull-apart basin (Wagreich and Decker, 2001). We therefore see evidence that marine – non-marine cycles in the Grünbach Formation may have had primarily a climatic control.

6. CONCLUSIONS

Geochemical parameters can be used to differentiate between marine and non-marine parts of Upper Cretaceous cycles. Marine and non-marine cycle parts can be recognized using boron concentrations and B/Al* ratios in combination with stable carbon isotope ratios. A significant differentiation is present for the ratio B/Al* and absolute boron concentrations after exclusion of coal layers, which have strongly different geochemical characteristics. The aluminium normalized boron ratio is more robust to lithological changes. $\delta^{13}\text{C}$ ratios of marine intervals are higher than those of non-marine intervals. Generally, the combination of different geochemical parameters is useful for the interpretation of the paleosalinity.

Five non-marine – marine cycles, with an estimated cycle mean duration of several 100 kyr are recognized in the trench section. Low subsidence rates and uniform provenance data are in favor of a climatic origin of third-order terrestrial-marine (transgressive-regressive) cycles in the Early Campanian.

ACKNOWLEDGEMENTS

This work was sponsored by a cooperation project of OMV F&E and the University of Vienna (FA536004). We thank OMV E&P and Philipp Strauss for continuous support. G. Hofer acknowledges a DOC-fellowship of the Austrian Academy of Sciences. Maria Heinrich and Albert Schedl (Geological Survey of Austria) are acknowledged for the possibility to use the old mining documentations in surveys archive. We thank Agrargemeinschaft Maiersdorf and especially its chairman Gerald Wöhrer for the permission to dig the trench and logistic support. Excavation and backfill has been carried out by Ing. Hermann Halbwies GmbH in Maiersdorf. Field work was supported by UNESCO-IGCP 555 "Rapid Environmental/Climate Change in the Cretaceous Greenhouse World: Ocean-Land Interactions" and the Austrian Academy of Sciences. We acknowledge Philipp Strauss, Gerhard Arzmüller, Godfrid Wessely, Herbert Summesberger and Leopold Krystyn for discussion and Ulli Exner for support with differential GPS. Interpretation and drawing of structural data has been carried out by Geocalculator 4.9 (written by Rod Holcombe) and Stereo32 1.0.3 (written by Klaus Röller, Bochum). This manuscript benefited from two anonymous reviews of an earlier version and reviews and editorial remarks by Herbert Summesberger and Martin Zuschin.

REFERENCES

- Berner, R.A. and Raiswell, R., 1984. C/S method for distinguishing freshwater from marine sedimentary rocks. *Geology*, 12, 365-368.
- Bornemann, A., Norris, R.D., Friedrich, O., Beckmann, B., Schouten, S., Sinninghe Damsté, J.S., Vogel, J., Hofmann, T. and Wagner, T., 2008. Isotopic evidence for glaciation during the Cretaceous Supergreenhouse. *Science*, 319, 189-192.
- Buggle, B., Glaser, B., Hambach, U., Gerasimenko, N. and Marković, S., 2011. An evaluation of geochemical weather indices in loess-paleosol studies. *Quaternary International*, 240, 12-21.
- Burnett, J.A., with contributions from Gallagher, L.T., Hampton, M.J., 1998. Upper Cretaceous. In: P.R. Bown (ed.), *Calcareous Nannofossil Biostratigraphy*. British Micropalaeontological Society Publications Series, Chapman and Hall, London, pp. 132-199.
- Clayton, R.N. and Degens, E.T., 1959. Use of carbon isotope analyses of carbonates for differentiating freshwater and marine sediments. *American Association of Petroleum Geologists Bulletin*, 43, 890-897.
- Cullers, R.L., 2000. The geochemistry of shales, siltstones and sandstones of Pennsylvanian-Permian age, Colorado, USA: implications for provenance and metamorphic studies. *Lithos*, 51, 181-203.
- Dominik, J. and Stanley, D.J., 1993. Boron, beryllium and sulfur in Holocene sediments and peats of the Nile delta, Egypt: their use as indicators of salinity and climate. *Chemical Geology*, 104, 203-216.
- Draxler, I., 1997. Postconference Excursion: 2.2.2.1. Palynological contribution on the coal-bearing Series of Grünbach. *Excursion Guides, Climates: Past, Present and Future*, Second European Palaeontological Congress, Vienna 10-12 July 1997, 80-89.
- Ernst, W., 1966. Stratigraphisch-fazielle Identifizierung von Sedimenten auf chemisch-geologischem Wege. *International Journal of Earth Sciences*, 55, 21-29.
- Fedo, C.M., Young, G.M. and Nesbitt, G.M., 1997. Paleoclimatic control on the composition of the Paleoproterozoic Serpent Formation, Huronian Supergroup, Canada: A greenhouse to icehouse transition. *Precambrian Research*, 86, 201-223.
- Forster, A., Schouten, S., Baas, M. and Sinninghe Damsté, J.S., 2007. Mid-Cretaceous (Albian-Santonian) sea surface temperature record of the tropical Atlantic Ocean. *Geology*, 35, 919-922.
- Gale, A.S., Hardenbol, J., Hathaway, B., Kennedy, W.J., Young, J.R. and Phansalkar, V., 2002. Global correlation of Cenomanian (Upper Cretaceous) sequences: evidence for Milankovitch control on sea level. *Geology*, 30, 291-294.
- Garver, J.I., Royce, P.R. and Smick, T.A., 1996. Chromium and nickel in shale of the Taconic foreland: a case study for the provenance of fine-grained sediments with an ultramafic source. *Journal of Sedimentary Research*, 66, 100-106.
- Glasspool, I.J., 2003. Hypautochthonous-allochthonous coal deposition in the Permian, South African, Witbank Basin No. 2 seam; a combined approach using sedimentology, coal petrology and palaeontology. *International Journal of Coal Geology*, 53, 81-135.
- Heling, D., 1967. Die Salinitätsfazies von Keupersedimenten aufgrund von Borgehaltsbestimmungen. *Sedimentology*, 8, 63-72.
- Herm, D., 1977. Zyklische Regressions-Sedimentation und Fossil-Vergesellschaftungen in der Gosau (Santonium) von Brandenberg/Tirol. *Mitteilungen der Bayerischen Staatssammlung für Paläontologie und Historische Geologie*, 17, 257-277.
- Hudson, J.D., 1977. Stable isotopes and limestone lithification. *Journal of the Geological Society of London*, 133, 637-660.

- ICCP, 1998. The New Vitrinite Classification (ICCP System 1994). *Fuel*, 77, 349-358.
- ICCP, 2001. The New Inertinite Classification (ICCP System 1994). *Fuel*, 80, 459-471.
- Ivanova, A.V. and Zaitseva, L.B., 2006. Influence of oxidability of carboniferous coals from the Dobrudja foredeep on vitrinite reflectance. *Lithology and Mineral Ressources*, 41/5, 435-439.
- Jenkyns, H.C., 2003. Evidence for rapid climate change in the Mesozoic-Palaeogene greenhouse world. *Philosophical Transactions of the Royal Society, Series A* 361, 1885-1916.
- Kreiner, H., 1994. Der Grünbacher Steinkohlenbergbau und seine Zeit 1823-1965. 2. Auflage, Marktgemeinde Grünbach, Grünbach, 376 pp.
- Locklair, R.E. and Sageman, B.B., 2008. Cyclostratigraphy of the Upper Cretaceous Niobrara Formation, Western Interior, U.S.A.: A Coniacian-Santonian orbital timescale. *Earth and Planetary Science Letters*, 269, 540-553.
- McCabe, P.J. and Parrish, J.T., 1992. Tectonic and climatic controls on the distribution and quality of Cretaceous coals. In: P.J. McCabe and J.T. Parrish (eds.), Controls on the distribution and quality of Cretaceous coals. Geological Society of America Special Paper, 267, pp. 1-15.
- McLennan, S.M., 1993. Weathering and global denudation. *Journal of Geology*, 101, 295-303.
- McLennan, S.M., Hemming, S., McDaniel, D.K. and Hanson, G.M., 1993. Geochemical approaches to sedimentation, provenance, and tectonics. In: M.J. Johnsson and A. Basu (eds.), Processes Controlling the Composition of Clastic Sediments. Geological Society of America Special Papers 284, pp. 21-40.
- Miller, K.G., Kominz, M.A., Browning, J.V., Wright, J.D., Mountain, G.S., Katz, M.E., Sugarman, P.J., Cramer, B.S., Christie-Blick, N. and Pekar, S.F., 2005a. The Phanerozoic record of global sea-level change. *Science*, 310, 1293-1298.
- Miller, K.G., Wright, J.D. and Browning, J.V., 2005b. Visions of ice sheets in a greenhouse world. *Marine Geology*, 217, 215-231.
- Miller, K.G., Wright, J.D., Katz, M.E., Browning, J.V., Cramer, B.S., Wade, B.S. and Mizintseva, S.F., 2008. A view of Antarctic ice-sheet evolution from sea-level and deep-sea isotope changes during the Late Cretaceous-Cenozoic. In: A.K. Cooper, P.J. Barrett, H. Stagg, B. Storey, E. Stump, W. Wise and the 10th ISAES editorial team (eds.), *Antarctica: A keystone in a changing world: Proceedings of the 10th International Symposium on Antarctic Earth Sciences*. The National Academies Press, Washington DC, pp. 55-70.
- Mizintseva, S.F., Browning, J.V., Miller, K.G., Olsson, R.K. and Wright, J.D., 2009. Integrated Late Santonian-Early Campanian sequence stratigraphy, New Jersey Coastal Plain: Implications for global sea-level studies. *Stratigraphy*, 6, 45-60.
- Müller, G. and Gastner, M., 1971. The „Karbonat-Bombe“, a simple device for the determination of the carbonate content in sediments, soils, and other materials. *Neues Jahrbuch für Mineralogie Monatshefte*, 10, 466-469.
- Nesbitt, H.W. and Young, G.M., 1982. Early Proterozoic climates and plate motions inferred from major element chemistry of lutites. *Nature*, 299, 715-717.
- Nesbitt, H.W. and Young, G.M., 1989. Formation and diagenesis of weathering profiles. *Journal of Geology*, 97, 129-147.
- Norris, R.D., Bice, K.L., Magno, E.A. and Wilson, P.A., 2002. Jiggling the tropical thermostat in the Cretaceous hothouse. *Geology*, 30, 299-302.
- Ogg, J.G., Agterberg, F.P. and Gradstein, F.M., 2004. The Cretaceous Period. In: F.M. Gradstein, F.P. Agterberg and A.G. Smith (eds.). *A Geologic Time Scale 2004*, Cambridge University Press, Cambridge, pp. 344-383.
- Plöchinger, B., 1961. Die Gosaumulde von Grünbach und der Neuen Welt. *Jahrbuch der Geologischen Bundesanstalt*, 104, 359-441.
- Plöchinger, B., 1967. Erläuterungen zur Geologischen Karte des Hohe Wand-Gebietes (Niederösterreich). *Geologische Bundesanstalt, Wien*, 142 pp.
- Rákosi, L. and Barbacka, M., 1999/2000. Upper Cretaceous flora from Ajka (W Hungary). I. Thallophyta. *Studia Botanica Hungarica*, 30/31, 27-55.
- Reinhardt, E.G., Fitton, R.J. and Schwarcz, H.P., 2003. Isotopic (Sr, O, C) indicators of salinity and taphonomy in marginal marine systems. *Journal of Foraminiferal Research*, 33, 262-272.
- Roser, B.P. and Korsch, R.J., 1988. Provenance signatures of sandstone-mudstone suites determined using discriminant function analysis of major-element data. *Chemical Geology*, 67, 119-139.
- Rügner, O., 2000. Tonmineral-Neubildung und Paläosalinität im Unteren Muschelkalk des südlichen Germanischen Beckens. Unpublished PhD thesis, University of Heidelberg, Heidelberg, 189 pp.
- Sachsenhofer, R., 1987. Fazies und Inkohlung mesozoischer Kohlen der Alpen Ostösterreichs. *Mitteilungen der Österreichischen Geologischen Gesellschaft*, 80, 1-45.

- Sageman, B.B. and Lyons, T.W., 2004. Geochemistry of Fine-grained Sediments and Sedimentary Rocks. In: F. MacKenzie (ed.), Sediments, Diagenesis, and Sedimentary Rocks, Treatise on Geochemistry, 7, pp. 115-158.
- Sanders, D., 1998. Tectonically controlled Late Cretaceous terrestrial to neritic deposition (Northern Calcareous Alps, Tyrol, Austria). *Facies*, 39, 139-178.
- Scarby, A., 1986. Normapolles anthers from the Upper Cretaceous of southern Sweden. *Review of Palaeobotany and Palynology*, 46, 235-256.
- Schlagintweit, F. and Wagreich, M., 1992. Über ein Vorkommen von *Munieria grambasti sarda* CHERCHI et al. in der obersantonen-untercampanen Gosau Gruppe des Miesenbachtales (Niederösterreich). *Mitteilungen der Gesellschaft der Geologie- und Bergbaustudenten in Österreich*, 38, 21-29.
- Schrank, E. and Ibrahim, M.I.A., 1995. Cretaceous (Aptian-Maastrichtian) palynology of foraminifera dated wells (KRM-1, AG-18) in northwestern Egypt. *Berliner Geowissenschaftliche Abhandlungen, Reihe A*, 177, 1-44.
- Schulz, O. and Fuchs, H.W., 1991. Kohle in Tirol: Eine historische, kohlenpetrologische und lagerstättenkundliche Betrachtung. *Archiv für Lagerstättenforschung der Geologischen Bundesanstalt*, 13, 123-213.
- Selter, V., David, F. and Kraft, T., 1989. Zusammenhänge zwischen Fazies und Borgehalten im nordwestdeutschen Oberkarbon-Becken. *Geologisch-Paläontologische Mitteilungen Innsbruck*, 16, 108-111.
- Spötl, C. and Vennemann, T., 2003. Continuous-flow IRMS analysis of carbonate minerals. *Rapid Communications in Mass Spectrometry*, 17, 1004-1006.
- Summesberger, H., 1997. The Cretaceous of the Grünbach - Neue Welt Basin. In: W.E. Piller, H. Summesberger, I. Draxler, M. Harzhauser and O. Mandic (eds.), Meso- to Cenozoic tropical/subtropical climates – Selected examples from the Northern Calcareous Alps and the Vienna Basin. *Excursion Guides Second European Palaeontological Congress Climates: Past, Present and Future*, Vienna 1997, Postconference Excursion, 2, pp. 77-89.
- Summesberger, H., Wagreich, M., Tröger, K.A. and Scholger, R., 2000. Piesting-Formation, Grünbach-Formation und Maiendorf-Formation – drei neue lithostratigraphische Termini in der Gosau Gruppe (Oberkreide) von Grünbach und der Neuen Welt (Niederösterreich). In: W.E. Piller (ed.), *Astrostrat 2000*. 24-26 November 2000 Gossendorf. *Vortragskurzfassungen und Exkursionsführer, Berichte des Institutes für Geologie und Paläontologie der Karl-Franzens-Universität Graz/Austria*, 2, pp. 23.
- Summesberger, H., Wagreich, M., Tröger, K.A. and Scholger, R., 2002. The Upper Cretaceous of Piesting (Austria): Integrated stratigraphy of the Piesting Formation (Gosau Group). In: M. Wagreich (ed.), *Aspects of Cretaceous Stratigraphy and Palaeobiogeography*. *Schriftenreihe der Erdwissenschaftlichen Kommission*, 15, pp. 373-399.
- Summesberger, H., Machalski, M. and Wagreich, M., 2007. First record of the late Campanian heteromorph ammonite *Nostoceras hyatti* from the Alpine Cretaceous (Grünbach, Go-sau Group, Lower Austria). *Acta Geologica Polonica*, 57, 443-451.
- Talbot, M.R., 1990. A review of the palaeohydrological interpretation of carbon and oxygen isotopic ratios in primary lacustrine carbonates. *Chemical Geology (Isotope Geoscience Section)*, 80, 261-279.
- Taylor, G.H., Teichmüller, M., Davis, A., Diessel, C.F.K., Littke, R. and Robert, P., 1998. *Organic Petrology*. Gebrüder Bornträger, Berlin, 198 pp.
- Teller, J.T., Glennie, K.W., Lancaster, N. and Singhvi, A.K., 2000. Calcareous dunes of the United Arab Emirates and Noah's Flood: the postglacial reflooding of the Persian (Arabian) Gulf. *Quaternary International*, 68-71, 297-308.
- Veizer, J., 1983. Trace Elements and Isotopes in Sedimentary Carbonates. In: R.J. Reeder (ed.), *Carbonates, mineralogy and chemistry. Reviews in Mineralogy and Geochemistry*, 11, pp. 265-299.
- Voigt, S. and Schönfeld, J., 2010. Cyclostratigraphy of the reference section for the Cretaceous white chalk of northern Germany, Lägerdorf-Kronsmoor: A late Campanian–early Maastrichtian orbital time scale. *Palaeogeography, Palaeoclimatology, Palaeoecology*, 287, 67-80.
- Wagreich, M., 1993. Subcrustal tectonic erosion in orogenic belts - A model for the Late Cretaceous subsidence of the Northern Calcareous Alps (Austria). *Geology*, 21, 941-944.
- Wagreich, M. and Faupl, P., 1994. Palaeogeography and geo-dynamic evolution of the Gosau Group of the Northern Calcareous Alps (Late Cretaceous, Eastern Alps, Austria). *Palaeogeography, Palaeoclimatology, Palaeoecology*, 110, 235-254.
- Wagreich, M. and Decker, K., 2001. Sedimentary tectonics and subsidence modelling of the type Upper Cretaceous Gosau basin (Northern Calcareous Alps, Austria). *International Journal of Earth Sciences*, 90, 714-726.
- Wagreich, M., Hu, X. and Sageman, B., 2011. Causes of oxic-anoxic changes in Cretaceous marine environments and their implications for Earth systems. *Sedimentary Geology*, 235, 1-4.
- Wagreich, M. and Krenmayr, H.G., 2005. Upper Cretaceous oceanic red beds (CORB) in the Northern Calcareous Alps (Nierental Formation, Austria): slope topography and clastic input as primary controlling factors. *Cretaceous Research*, 26, 57-64.

Yan, D., Chen, D., Wang, Q. and Wang, J., 2010. Large-scale climatic fluctuations in the latest Ordovician on the Yangtze block, south China. *Geology*, 38, 599-602.

For online Appendix and supplementary material to this publication see: www.univie.ac.at/ajes/archive/volume_104_2/

Received: 11 November 2011
Accepted: 13 December 2011

Gerald HOFER¹⁾, Erich DRAGANITS^{1,2)}, Michael WAGREICH¹⁾, Christa-Charlotte HOFMANN³⁾, Doris REISCHENBACHER⁴⁾, Marie-Louise GRUNDTNER¹⁾ & Magda BOTTIG⁵⁾

¹⁾ Department of Geodynamics and Sedimentology, University of Vienna, Althanstrasse 14, A-1090 Vienna, Austria;

²⁾ Department of Prehistoric and Medieval Archaeology, University of Vienna, Franz-Klein-Gasse 1, 1190 Vienna, Austria;

³⁾ Department of Palaeontology, University of Vienna, Althanstrasse 14, A-1090 Vienna, Austria;

⁴⁾ Department of Applied Geological Sciences and Geophysics, Montanuniversität Leoben, Franz-Joseph-Strasse 18, A-8700 Leoben, Austria;

⁵⁾ Geological Survey of Austria, Neulinggasse 38, A-1030 Vienna, Austria;

¹⁾ Corresponding author, gerald.hofer@univie.ac.at

APPENDIX**APPENDIX A**

Table of maceral analysis (classification of huminites, liptinites, inertinites and matrix) of coal particles for the samples M5, M8A, M14 and M17.

	particles M-5	particles M-8A	coal M-14	coal M-17
Huminite/Vitrinite				
Telinite				
Collotelinite	277	141	291	54
Corpogelinite				
Detrovitritinite				10
Collodetrinitrite				161
Phyllovitritinite				14
Sum Huminite	277	141	291	239
Liptinite				
Sporinite				2
Cutinite				12
Resinite	12			
Liptodetrinitrite				8
Alginite				5
Fluorinitite				3
Sum Liptinite	12	0	0	30
Inertinite				
Pyrofusinitite				4
Degradofusinitite				2
Funginitite				
Inertodetrinitrite				2
Sum Inertinite	0	0	0	8
Matrix				
Pyrite			8	9
Shale	11	11		10
Sum Matrix	11	19	9	23
	Σ	300	160	300
	%	100	100	100
Rr [%]	0.52	0.50	0.52	0.50
s	0.01	0.01	0.01	0.01
n	25	16	25	18

Maceral abundance M-5

mineral matter free

95.8 % Telovitritinite
0.0 % Detrovitritinite
0.0 % Gelovitritinite
95.8 % Vitrinite
4.2 % Liptinite
0.0 % Inertinite

Maceral abundance M-8a

mineral matter free

100.0 % Telovitritinite
0.0 % Detrovitritinite
0.0 % Gelovitritinite
100.0 % Vitrinite
0.0 % Liptinite
0.0 % Inertinite

Maceral abundance M-17

mineral matter free

19.5 % Telovitritinite
66.8 % Detrovitritinite
0.0 % Gelovitritinite
86.3 % Vitrinite
10.8 % Liptinite
2.9 % Inertinite

Maceral abundance M-14

mineral matter free

100.0 % Telovitritinite
0.0 % Detrovitritinite
0.0 % Gelovitritinite
100.0 % Vitrinite
0.0 % Liptinite
0.0 % Inertinite

TABLE 1

APPENDIX B

Geochemistry data. List of the sample set (M1-M92) from the Maiersdorf-trench. Analyzed geochemistry (major element oxides: SiO₂, Al₂O₃, Fe₂O₃, MgO, CaO, Na₂O, K₂O, TiO₂, P₂O₅, MnO and Cr₂O₃, minor elements: Ba, Be, Co, Cs, Ga, Hf, Nb, Ni, Rb, Sn, Sr, Ta, Th, U, V, W and Zr, noble and base metals: Mo, Cu, Pb, Zn, Ni, As, Cd, Sb, Bi, Ag, Au, Hg, Tl and Se, rare earth elements: Sc, Y, La, Ce, Pr, Nd, Sm, Eu, Gd, Tb, Dy, Ho, Er, Tm, Yb and Lu, loss on ignition: LOI, total C and S, total organic carbon: TOC, carbonate: CaCO₃, some elemental ratios: B/Al*, Th/U, Cr/Ni, Cr/V, Y/Ni, TOC/S, indices of alteration:

CIA and CPA and stable carbon and oxygen isotope ratios: δ¹³C and δ¹⁸O. The interpreted facies determinations (marine or non-marine) used for statistic calculations are added.

Samples of the Maiersdorf-trench

Sample-Nr.	SiO ₂ [%]	Al ₂ O ₃ [%]	Fe ₂ O ₃ [%]	MgO [%]	CaO [%]	Na ₂ O [%]	K ₂ O [%]	TiO ₂ [%]	P ₂ O ₅ [%]	MnO [%]	Cr ₂ O ₃ [%]	LOI [%]	Sum [%]	Sc [ppm]	Ba [ppm]	Be [ppm]
M-1	24.81	12.75	7.18	0.88	1.28	0.18	2.24	0.51	0.06	0.05	0.012	49.8	99.77	16	1473	4
M-1B	5.94	2.59	3.75	0.42	9.52	0.06	0.49	0.12	0.04	0.17	0.008	73.0	96.09	5	86	0
M-2																
M-3	65.44	17.06	5.12	1.48	0.31	0.50	3.81	0.97	0.20	0.03	0.014	4.9	99.83	16	622	3
M-4																
M-5	27.00	9.26	12.98	1.13	5.56	0.24	1.96	0.47	0.08	0.10	0.009	41.1	99.89	13	290	2
M-6	52.87	23.42	5.92	2.12	0.94	0.38	4.56	1.07	0.08	0.13	0.020	8.3	99.83	24	628	3
M-7	46.62	18.05	7.23	2.13	4.62	0.43	3.96	0.85	0.11	0.09	0.017	15.7	99.84	20	524	2
M-8B																
M-9A																
M-9B	49.69	26.47	3.61	1.82	1.29	0.31	4.03	1.17	0.08	0.03	0.023	11.3	99.83	27	598	4
M-12	42.38	16.56	7.55	1.40	1.59	0.35	3.44	0.77	0.09	0.06	0.015	25.7	99.87	18	441	3
M-13																
M-16	52.92	22.29	6.03	2.40	1.35	0.40	4.72	1.04	0.11	0.17	0.020	8.4	99.82	23	637	2
M-17	11.72	6.01	5.68	0.48	1.95	0.12	1.29	0.23	0.06	0.06	0.005	72.3	99.94	7	183	1
M-18	51.43	19.54	6.68	2.44	3.00	0.48	4.31	0.89	0.12	0.11	0.017	10.8	99.83	20	533	3
M-20																
M-23	52.93	14.82	5.31	2.24	8.56	0.62	3.26	0.83	0.14	0.10	0.011	11.0	99.85	14	480	0
M-24	53.20	23.58	5.91	2.26	0.43	0.42	4.88	1.07	0.09	0.14	0.019	7.8	99.82	24	661	4
M-25																
M-27																
M-31	52.73	22.21	4.93	2.42	2.63	0.46	5.04	1.02	0.11	0.03	0.019	8.2	99.83	22	612	4
M-33	66.30	14.72	4.02	1.65	0.75	0.71	2.95	0.85	0.31	0.02	0.016	7.6	99.87	15	430	2
M-36																
M-37	54.91	21.26	6.33	2.34	1.32	0.45	4.76	1.00	0.12	0.11	0.018	7.2	99.83	21	668	2
M-41																
M-42	66.58	15.37	5.40	1.90	0.49	0.50	3.19	0.97	0.15	0.07	0.014	5.2	99.84	15	491	2
M-46	45.05	19.72	7.66	2.96	6.50	0.39	4.35	0.91	0.13	0.16	0.016	12.0	99.83	21	551	4
M-48	53.49	18.86	6.09	2.23	4.23	0.40	4.27	0.94	0.13	0.09	0.015	9.1	99.84	19	534	2
M-50	54.17	20.93	4.96	2.14	2.89	0.52	4.64	1.01	0.10	0.05	0.016	8.4	99.83	20	624	4
M-53	54.77	21.65	6.34	2.33	0.74	0.32	4.76	1.00	0.06	0.07	0.019	7.8	99.84	22	593	3
M-55																
M-57	54.84	17.95	5.69	1.94	4.72	0.52	3.93	0.94	0.11	0.16	0.014	9.0	99.85	18	526	1
M-60	34.06	11.20	17.19	1.11	10.04	0.27	2.24	0.54	0.08	0.09	0.010	23.1	99.90	14	292	3
M-62																
M-64																
M-65	48.60	19.90	4.40	2.21	6.88	0.55	4.77	0.80	0.09	0.04	0.019	11.6	99.85	19	562	4
M-66																
M-67	31.01	11.89	6.05	0.63	3.87	0.28	2.15	0.47	0.06	0.08	0.010	43.4	99.92	13	315	5
M-68	50.54	24.07	4.71	1.23	1.91	0.33	4.85	1.06	0.05	0.00	0.021	11.1	99.86	25	641	2
M-69	54.83	14.52	7.36	1.65	7.27	0.53	3.07	0.80	0.14	0.17	0.013	9.5	99.86	16	434	2
M-71																
M-72	49.87	16.59	6.49	1.91	7.99	0.46	3.64	0.81	0.13	0.13	0.016	11.8	99.86	18	490	3
M-73																
M-74	21.87	9.17	8.19	0.76	5.56	0.20	1.86	0.37	0.06	0.02	0.009	51.8	99.93	13	263	3
M-75	47.03	15.14	7.24	1.72	10.27	0.51	3.44	0.76	0.13	0.12	0.015	13.5	99.86	16	450	2
M-77	46.04	14.16	5.39	1.52	13.31	0.49	3.09	0.77	0.15	0.14	0.012	14.8	99.87	15	449	3
M-78	50.48	17.53	4.39	1.85	7.95	0.49	3.76	0.85	0.12	0.11	0.015	12.3	99.86	17	539	2
M-79	43.42	13.48	15.62	1.14	1.60	0.43	2.80	0.70	0.09	0.03	0.015	20.5	99.88	16	416	5
M-82																
M-84	44.13	14.35	5.34	1.64	14.33	0.47	3.11	0.72	0.14	0.10	0.012	15.5	99.87	14	441	1
M-85																
M-87																
M-88	28.35	10.62	10.05	0.80	4.48	0.21	1.73	0.46	0.09	0.10	0.014	43.0	99.92	14	263	6
M-89																
M-90	60.27	18.26	3.66	1.72	2.99	0.41	3.26	0.95	0.08	0.02	0.018	8.2	99.86	18	456	2
M-92	49.67	19.69	5.94	2.08	6.07	0.45	4.15	0.90	0.11	0.12	0.016	10.7	99.85	19	575	2

TABLE 2

Samples of the Maiersdorf-trench

Sample-Nr.	Co [ppm]	Cs [ppm]	Ga [ppm]	Hf [ppm]	Nb [ppm]	Rb [ppm]	Sn [ppm]	Sr [ppm]	Ta [ppm]	Th [ppm]	U [ppm]	V [ppm]	W [ppm]	Zr [ppm]	Y [ppm]	La [ppm]
M-1	16.7	14.6	16.4	2.1	8.5	96.3	1	127.1	0.4	7.6	9.1	117	2.0	88.2	22.3	19.2
M-1B	7.2	1.6	12.3	0.9	9.4	20.4	0	255.4	0.1	2.3	4.0	260	3.6	35.0	8.3	5.7
M-2																
M-3	10.5	7.3	21.4	6.5	16.9	139.5	4	89.1	1.3	12.4	3.0	137	2.9	252.6	32.1	43.0
M-4																
M-5	17.3	4.9	14.0	2.6	8.4	73.0	2	191.1	0.5	6.3	4.4	76	2.5	104.0	21.2	19.8
M-6	22.2	14.3	29.0	4.8	17.9	188.8	5	101.2	1.4	14.2	4.6	199	2.9	164.5	30.0	37.5
M-7	19.1	11.2	23.9	4.0	15.5	154.6	4	179.4	1.1	11.9	5.9	163	2.2	145.8	30.8	30.9
M-8B																
M-9A																
M-9B	28.3	19.2	32.6	5.4	21.0	181.5	6	121.5	1.6	16.7	8.7	236	3.1	183.1	28.0	39.6
M-12	16.6	9.0	21.0	3.9	13.5	133.6	3	112.9	1.0	10.1	4.4	159	2.2	133.4	23.4	28.6
M-13																
M-16	24.5	12.3	27.9	4.6	18.1	182.5	5	124.6	1.2	13.6	3.6	189	2.7	154.9	28.7	36.6
M-17	7.2	3.9	9.0	0.9	4.5	52.6	1	149.2	0.2	2.9	8.2	98	1.0	38.1	13.0	10.2
M-18	20.2	12.2	24.5	4.3	16.3	159.6	4	135.9	1.2	13.8	4.2	147	2.7	149.8	27.3	33.4
M-20																
M-23	14.9	7.3	19.0	5.4	14.7	122.0	3	139.3	0.9	11.1	3.2	135	2.6	189.0	28.8	32.6
M-24	27.0	12.8	31.4	5.1	19.1	199.3	5	105.0	1.2	16.3	4.2	219	3.4	177.2	30.9	43.0
M-25																
M-27																
M-31	18.7	12.5	29.6	4.6	17.8	199.3	5	124.6	1.2	13.6	3.5	199	2.9	177.8	30.1	37.3
M-33	15.2	7.5	19.0	4.9	15.2	129.6	3	86.7	1.1	10.6	3.6	125	2.6	194.9	31.4	40.4
M-36																
M-37	17.6	11.4	27.1	5.0	16.9	190.5	6	101.7	1.1	16.0	3.2	189	2.7	178.9	31.8	39.2
M-41																
M-42	21.2	7.5	19.9	7.0	17.1	126.6	4	69.4	1.2	12.5	3.6	146	2.7	271.5	33.4	37.9
M-46	23.0	10.1	25.8	3.9	16.0	168.4	4	136.5	0.8	13.1	3.9	174	2.2	138.4	28.8	35.4
M-48	22.7	10.6	24.1	4.9	16.3	168.1	5	112.5	1.1	13.3	3.4	157	2.7	178.8	32.2	37.3
M-50	23.6	13.0	27.5	5.5	18.1	202.5	5	94.5	1.1	15.3	3.9	185	2.8	185.9	32.4	42.0
M-53	27.2	13.7	28.6	5.2	18.2	196.3	5	92.1	1.3	15.7	3.2	181	2.7	170.5	28.5	39.8
M-55																
M-57	22.4	10.3	22.9	5.9	16.4	156.9	4	85.3	1.1	13.1	3.4	144	2.6	210.3	33.4	39.0
M-60	12.5	7.0	16.1	3.1	10.2	92.7	3	129.5	0.7	9.3	4.5	106	2.3	116.3	25.4	24.8
M-62																
M-64																
M-65	19.4	15.5	25.4	4.2	15.9	198.8	5	94.8	1.1	14.7	3.0	133	3.6	152.8	23.9	34.9
M-66																
M-67	27.2	7.5	15.3	2.6	7.5	89.5	3	67.6	0.5	6.8	3.4	93	2.0	103.1	29.6	21.3
M-68	3.2	21.8	32.6	4.9	18.9	216.6	5	92.2	1.3	17.4	3.7	203	3.2	166.3	24.1	41.6
M-69	18.3	7.4	18.0	4.8	14.1	115.2	3	119.9	0.9	10.4	2.7	116	2.4	182.4	31.2	32.9
M-71																
M-72	24.3	10.2	20.2	4.4	14.3	143.3	4	122.8	1.0	12.4	2.8	149	2.1	153.2	31.0	35.4
M-73																
M-74	7.0	6.8	17.1	2.0	7.1	77.7	2	72.4	0.4	6.9	3.7	90	2.9	71.9	23.0	17.1
M-75	19.9	10.6	19.4	4.9	14.2	137.5	3	145.4	0.8	11.3	3.1	121	2.2	165.3	28.2	34.5
M-77	17.2	8.0	18.4	5.3	14.1	121.8	3	137.3	0.8	11.9	3.2	114	2.7	163.5	28.8	32.5
M-78	18.6	10.9	21.9	4.7	15.0	154.9	4	91.0	1.0	13.3	3.6	148	2.6	157.3	27.6	35.1
M-79	17.8	8.4	18.8	4.4	12.8	112.5	3	61.1	0.9	10.7	5.4	172	2.1	165.7	28.6	30.7
M-82																
M-84	17.6	10.1	17.7	4.1	13.2	126.3	3	140.8	0.7	10.8	2.6	119	2.4	143.6	25.6	30.0
M-85																
M-87																
M-88	16.2	23.5	15.7	2.6	8.1	86.0	2	66.1	0.6	7.2	3.4	111	2.1	100.9	27.9	22.0
M-89																
M-90	23.4	15.0	22.3	5.2	15.8	149.4	4	73.7	1.0	12.5	3.0	146	2.8	186.5	28.6	36.5
M-92	23.6	11.3	24.4	4.0	15.1	163.7	4	100.3	1.0	14.0	3.2	159	3.2	145.9	27.3	35.6

TABLE 2 CONTINUED

Samples of the Maiersdorf-trench

Sample-Nr.	Ce [ppm]	Pr [ppm]	Nd [ppm]	Sm [ppm]	Eu [ppm]	Gd [ppm]	Tb [ppm]	Dy [ppm]	Ho [ppm]	Er [ppm]	Tm [ppm]	Yb [ppm]	Lu [ppm]	TOT/C [%]	TOT/S [%]	Mo [ppm]
M-1	43.4	4.80	20.2	4.02	0.93	3.81	0.64	3.45	0.74	2.10	0.33	2.10	0.30	32.04	3.64	3.3
M-1B	13.3	1.54	5.7	1.36	0.34	1.40	0.27	1.41	0.30	0.84	0.15	0.84	0.14	49.65	0.13	1.0
M-2																
M-3	94.7	10.31	38.1	6.92	1.40	5.89	0.94	5.29	1.07	3.15	0.46	3.14	0.45	0.19	0.00	0.3
M-4																
M-5	45.0	5.11	22.2	4.23	0.97	4.09	0.68	3.72	0.70	2.07	0.33	1.94	0.28	24.72	4.83	5.9
M-6	79.0	8.94	35.3	6.48	1.39	5.56	0.93	5.38	1.09	3.18	0.51	3.22	0.46	0.63	0.11	0.2
M-7	66.9	7.54	31.5	6.04	1.35	5.53	0.91	5.27	1.01	2.94	0.45	3.00	0.44	6.38	3.00	2.3
M-8B																
M-9A																
M-9B	83.8	9.60	38.7	7.02	1.51	5.62	0.91	5.01	1.03	3.14	0.47	3.22	0.50	1.28	0.13	1.5
M-12	58.8	6.71	28.0	5.07	1.13	4.45	0.74	4.27	0.85	2.51	0.37	2.46	0.37	10.73	0.51	2.9
M-13																
M-16	75.7	8.51	33.7	6.37	1.37	5.31	0.92	5.19	1.05	3.05	0.46	3.21	0.44	0.88	0.07	0.6
M-17	23.4	2.67	10.5	2.23	0.52	2.46	0.38	2.03	0.39	1.09	0.16	0.91	0.16	48.96	0.25	5.6
M-18	72.3	7.91	30.8	6.30	1.37	5.36	0.88	4.76	0.94	2.85	0.44	2.83	0.42	2.64	0.98	1.1
M-20																
M-23	71.4	7.91	31.3	5.65	1.21	5.30	0.86	4.77	0.95	2.87	0.44	2.66	0.44	2.10	0.38	1.1
M-24	91.4	10.12	41.6	7.27	1.49	6.44	0.99	5.66	1.16	3.36	0.53	3.31	0.51	0.48	0.25	1.3
M-25																
M-27																
M-31	79.9	8.95	33.8	6.17	1.24	5.28	0.86	5.12	1.00	2.99	0.45	3.04	0.46	0.97	0.02	0.3
M-33	88.6	9.84	39.1	7.09	1.50	6.38	1.03	5.62	1.05	3.13	0.46	2.86	0.46	1.97	0.04	0.3
M-36																
M-37	86.8	9.72	36.8	6.93	1.38	6.05	0.96	5.68	1.08	3.29	0.51	3.26	0.50	0.34	0.00	1.0
M-41																
M-42	80.7	8.91	35.1	6.38	1.40	6.12	1.00	5.79	1.14	3.43	0.52	3.41	0.51	0.07	0.00	0.2
M-46	78.0	8.54	35.5	6.16	1.31	5.51	0.86	4.95	0.96	2.91	0.44	2.79	0.44	1.68	0.00	1.5
M-48	81.9	9.21	35.8	6.54	1.36	5.95	0.98	5.26	1.09	3.36	0.49	3.27	0.48	0.84	0.00	0.1
M-50	88.7	10.22	40.8	7.32	1.51	6.32	1.00	5.58	1.10	3.30	0.51	3.38	0.53	0.69	0.00	1.5
M-53	87.0	9.87	38.0	6.84	1.32	5.53	0.89	5.22	1.03	3.35	0.49	3.26	0.49	0.11	0.00	0.0
M-55																
M-57	83.3	9.61	36.8	6.87	1.44	6.27	1.01	5.99	1.15	3.45	0.51	3.25	0.51	0.99	0.00	0.2
M-60	54.2	6.36	25.6	4.92	1.14	5.03	0.79	4.36	0.89	2.60	0.38	2.44	0.38	7.53	0.13	10.6
M-62																
M-64																
M-65	73.8	8.52	32.8	5.77	1.11	4.89	0.75	4.49	0.89	2.56	0.40	2.54	0.40	1.53	0.00	0.6
M-66																
M-67	48.7	5.76	23.5	5.21	1.18	5.59	0.94	5.41	1.06	3.14	0.47	2.89	0.45	20.88	0.82	17.3
M-68	86.3	9.48	34.8	6.03	1.21	4.73	0.72	4.10	0.85	2.73	0.40	2.75	0.43	1.41	0.00	1.3
M-69	71.7	8.12	31.9	6.22	1.33	5.80	0.92	5.23	1.06	3.10	0.46	3.02	0.46	1.44	0.00	0.8
M-71																
M-72	77.8	8.65	32.8	6.60	1.35	6.26	0.98	5.49	1.07	3.07	0.45	2.96	0.45	1.79	0.00	1.2
M-73																
M-74	36.8	4.27	16.2	3.59	0.83	3.76	0.67	3.70	0.78	2.32	0.36	2.28	0.37	25.61	0.02	5.5
M-75	73.4	8.38	33.3	6.03	1.28	5.44	0.90	4.80	0.98	2.96	0.42	2.78	0.41	2.26	0.00	1.3
M-77	68.8	7.99	31.3	5.87	1.26	5.57	0.91	4.96	1.04	3.04	0.43	2.76	0.43	2.86	0.00	0.4
M-78	74.7	8.53	32.3	6.08	1.23	5.29	0.87	4.65	1.00	2.96	0.44	2.88	0.43	1.80	0.00	0.6
M-79	64.9	7.64	30.8	5.56	1.20	5.10	0.86	4.98	1.00	3.02	0.46	3.01	0.45	7.62	0.25	19.4
M-82																
M-84	65.3	7.24	29.3	5.37	1.07	4.79	0.78	4.38	0.88	2.61	0.40	2.62	0.38	3.07	0.00	0.7
M-85																
M-87																
M-88	45.7	5.44	22.4	4.54	1.03	4.78	0.77	4.47	0.87	2.55	0.38	2.48	0.38	21.43	0.66	5.6
M-89																
M-90	78.2	8.76	34.6	6.32	1.30	5.57	0.90	4.93	1.02	3.03	0.44	2.92	0.44	0.83	0.00	0.0
M-92	74.9	8.68	33.5	6.25	1.33	5.51	0.87	4.74	1.00	2.88	0.42	2.88	0.45	1.33	0.00	0.5

TABLE 2 CONTINUED

Samples of the Maiersdorf-trench

Sample-Nr.	Cu [ppm]	Pb [ppm]	Zn [ppm]	Ni [ppm]	As [ppm]	Cd [ppm]	Sb [ppm]	Bi [ppm]	Ag [ppm]	Au [ppb]	Hg [ppm]	Tl [ppm]	Se [ppm]	B [ppm]	B/Al*	¹³ C [VPDB]
M-1	37.9	9.6	70	38.5	34.4	0.2	1.3	0.3	0.0	1.1	1.54	0.0	2.1	132	196	-2.28
M-1B	7.6	4.5	13	12.4	40.5	0.0	4.8	0.0	0.0	0.0	1.25	0.0	0.6	187	1365	
M-2																-2.93
M-3	36.8	9.6	49	33.6	13.3	0.0	1.0	0.5	0.1	2.7	2.55	0.0	0.0	179	198	
M-4																-4.70
M-5	27.6	20.7	42	62.6	300.4	0.2	6.5	0.2	0.1	0.0	4.12	0.3	0.8	214	437	
M-6	65.3	15.6	55	40.3	3.4	0.0	0.3	0.5	0.1	2.8	0.27	0.0	0.5	225	182	
M-7	41.1	12.7	180	50.0	70.2	0.3	0.9	0.4	0.1	1.5	1.41	0.1	0.9	160	168	-2.04
M-8B																-3.04
M-9A																
M-9B	78.3	21.7	66	55.7	13.4	0.2	1.2	0.6	0.2	1.6	0.96	0.0	1.0	272	194	
M-12	37.6	15.9	55	56.4	59.3	0.1	4.4	0.4	0.0	1.1	2.38	0.1	2.0	146	167	
M-13																-2.88
M-16	64.4	12.5	53	51.5	5.9	0.0	0.4	0.5	0.0	2.8	0.34	0.0	0.0	179	152	
M-17	16.6	5.0	43	22.6	18.9	0.3	0.4	0.1	0.0	0.0	0.78	0.0	1.5	168	528	
M-18	51.6	10.6	50	51.6	24.2	0.1	0.6	0.5	0.1	0.9	0.71	0.0	0.0	164	159	-1.42
M-20																
M-23	40.6	7.5	43	38.4	17.3	0.0	0.7	0.3	0.0	1.0	0.71	0.0	0.5	146	186	-4.03
M-24	67.8	14.6	65	64.0	11.5	0.2	0.3	0.5	0.1	1.4	0.64	0.0	0.0	160	128	
M-25																
M-27																-3.21
M-31	55.3	16.3	49	49.0	9.6	0.0	0.7	0.5	0.0	1.1	0.66	0.0	0.0	178	151	
M-33	45.6	6.0	63	41.6	21.2	0.0	0.8	0.3	0.0	0.6	0.46	0.0	0.6	111	143	-7.19
M-36																
M-37	49.1	10.1	47	56.1	10.6	0.0	0.5	0.4	0.0	2.1	0.66	0.0	0.0	170	151	
M-41																
M-42	50.1	7.9	44	53.6	5.6	0.0	0.4	0.3	0.0	2.3	0.50	0.0	0.0	123	151	
M-46	54.7	12.4	62	53.5	11.7	0.2	0.6	0.4	0.0	2.1	0.51	0.0	0.0	167	160	-4.35
M-48	50.0	13.9	56	52.6	3.1	0.1	0.2	0.4	0.0	2.6	0.74	0.0	0.0	173	173	-5.67
M-50	58.3	17.7	62	51.8	32.5	0.0	0.9	0.4	0.0	1.2	1.66	0.0	0.0	163	147	
M-53	53.9	15.6	54	58.7	0.7	0.0	0.1	0.4	0.0	1.8	1.23	0.0	0.0	154	134	
M-55																-7.18
M-57	51.3	11.4	47	56.1	5.6	0.0	0.2	0.4	0.0	2.3	0.60	0.0	0.0	132	139	-9.03
M-60	26.0	9.9	39	60.7	128.4	0.3	2.6	0.2	0.1	0.0	2.22	0.2	0.8	89	150	-7.61
M-62																-3.69
M-64																-9.21
M-65	38.6	16.2	52	51.5	10.7	0.1	0.1	0.4	0.0	2.1	0.30	0.0	0.0	150	142	-5.83
M-66																-5.32
M-67	28.7	5.8	79	75.4	110.5	0.1	1.6	0.2	0.1	0.9	4.99	0.1	1.9	74	118	
M-68	28.8	25.2	6	5.1	33.9	0.0	0.5	0.5	0.2	3.5	1.85	0.1	0.0	190	149	-8.94
M-69	43.1	12.2	41	70.2	21.0	0.1	0.9	0.3	0.0	1.4	0.81	0.0	0.0	128	167	-4.60
M-71																-9.32
M-72	44.6	13.5	52	74.5	20.6	0.1	0.4	0.4	0.0	1.3	0.63	0.0	0.0	147	167	-5.82
M-73																-9.27
M-74	33.2	10.2	45	45.1	27.5	0.2	2.2	0.2	0.0	0.0	4.95	0.2	1.1	62	128	
M-75	37.1	15.9	63	68.5	41.0	0.2	1.0	0.4	0.0	2.1	1.26	0.0	0.0	133	166	-3.58
M-77	40.1	10.1	39	49.0	11.0	0.0	0.2	0.3	0.0	1.6	0.24	0.0	0.0	115	153	-5.85
M-78	42.1	8.8	41	68.8	26.9	0.2	0.1	0.4	0.0	1.4	0.48	0.0	0.0	139	150	-9.27
M-79	50.7	16.6	46	78.5	80.8	0.4	7.6	0.4	0.2	1.1	4.46	0.4	1.2	114	160	
M-82																-6.38
M-84	34.6	10.1	42	60.2	22.8	0.1	0.4	0.3	0.0	1.3	0.65	0.0	0.0	112	148	-6.36
M-85																0.28
M-87																-0.57
M-88	54.0	13.0	90	97.0	51.4	0.3	3.4	0.2	0.2	0.7	1.83	0.1	1.6	67	119	-3.29
M-89																
M-90	49.1	11.9	39	42.2	21.5	0.0	0.3	0.4	0.0	2.2	0.46	0.0	0.0	138	143	
M-92	49.3	11.6	52	63.0	14.9	0.0	0.3	0.4	0.0	1.9	0.53	0.0	0.0	148	142	-6.34

TABLE 2 CONTINUED

Samples of the Maiersdorf-trench

Sample-Nr.	$\delta^{18}\text{O}$ [VPDB]	TOC	CaCO_3 [%]	Th/U	Cr/Ni	Cr/V	Y/Ni	TOC/S	CIA	CPA	Interpreted facies
M-1		33.75	0	0.84	2.11	0.69	0.58	9.3	80.71	97.73	marine
M-1B				0.58	4.36	0.21	0.67		77.82	96.33	
M-2	-5.73	1.68	20								marine
M-3		0.15	0	4.13	2.82	0.69	0.96		74.45	95.40	marine
M-4	-5.67	1.80	16								marine
M-5	-6.42	26.30	17	1.43	0.97	0.80	0.34	5.4	75.82	95.91	
M-6		0.56	0	3.09	3.35	0.68	0.74	5.1	78.93	97.40	marine
M-7	-6.40	4.85	12	2.02	2.30	0.70	0.62	1.6	75.76	96.23	marine
M-8B			9								
M-9A	-5.84	0.09	13								marine
M-9B		1.06	4	1.92	2.79	0.66	0.50	8.2	82.96	98.11	marine
M-12		12.05	9	2.30	1.80	0.64	0.41	23.6	77.04	96.64	non-marine
M-13			0								
M-16	-5.27	0.62	10	3.78	2.62	0.72	0.56	8.8	77.44	97.13	non-marine
M-17		52.80	0	0.35	1.49	0.34	0.58	211.2	76.84	96.82	
M-18	-5.15	2.16	13	3.29	2.23	0.78	0.53	2.2	75.54	96.12	non-marine
M-20			0								
M-23	-5.97	0.35	20	3.47	1.94	0.55	0.75	0.9	72.31	93.56	marine
M-24		0.46	0	3.88	2.01	0.59	0.48	1.8	77.78	97.15	marine
M-25			4								
M-27	-6.51	1.72	11								marine
M-31		0.58	0	3.89	2.62	0.65	0.61	29.2	75.91	96.71	marine
M-33		2.09	9	2.94	2.60	0.86	0.75	52.3	72.26	92.65	non-marine
M-36	-8.41	0.12	20								non-marine
M-37		0.18	6	5.00	2.17	0.64	0.57		76.01	96.64	non-marine
M-41			0								
M-42		0.04	0	3.47	1.76	0.65	0.62		74.78	94.92	non-marine
M-46	-6.86	0.33	13	3.36	2.02	0.62	0.54		76.50	96.85	marine
M-48	-7.09	0.09	14	3.91	1.93	0.65	0.61		75.84	96.63	marine
M-50		0.19	4	3.92	2.09	0.58	0.63		75.41	96.07	non-marine
M-53		0.05	0	4.91	2.19	0.71	0.49		77.57	97.63	non-marine
M-55	-7.43	0.11	18								non-marine
M-57	-8.34	0.11	11	3.85	1.69	0.66	0.60		74.78	95.45	non-marine
M-60	-8.39	6.41	19	2.07	1.11	0.64	0.42	49.3	76.92	96.19	non-marine
M-62	-6.78	0.12	18								non-marine
M-64	-8.46	0.14	18								non-marine
M-65	-7.44	0.17	18	4.90	2.49	0.97	0.46		73.79	95.65	marine
M-66	-7.42	0.24	21								marine
M-67		21.45	0	2.00	0.90	0.73	0.39	26.2	78.29	96.27	
M-68	-10.01	1.36	11	4.70	27.82	0.70	4.73		79.01	97.79	marine
M-69	-6.37	0.08	17	3.85	1.25	0.76	0.44		73.79	94.34	marine
M-71	-8.85	1.89	14								marine
M-72	-7.04	0.24	18	4.43	1.45	0.73	0.42		74.99	95.64	marine
M-73	-9.03	0.98	12								marine
M-74		26.90	0	1.86	1.35	0.68	0.51	1345.0	77.21	96.54	
M-75	-6.49	0.17	22	3.65	1.48	0.84	0.41		73.39	94.75	marine
M-77	-7.48	0.13	25	3.72	1.65	0.71	0.59		73.74	94.61	non-marine
M-78	-8.71	0.25	19	3.69	1.47	0.68	0.40		75.25	95.60	non-marine
M-79		7.36	0	1.98	1.29	0.59	0.36	29.4	74.89	95.01	non-marine
M-82	-7.97	0.19	22								non-marine
M-84	-7.53	0.20	27	4.15	1.35	0.68	0.43		74.18	94.89	marine
M-85	-5.35										marine
M-87	-5.40	0.70	47								marine
M-88		21.45	5	2.12	0.98	0.85	0.29	32.5	80.33	96.85	
M-89	-6.98	0.48	26								marine
M-90		0.41	4	4.17	2.88	0.83	0.68		78.68	96.44	non-marine
M-92	-7.86	0.19	16	4.38	1.72	0.68	0.43		76.49	96.38	non-marine

TABLE 2 CONTINUED